

Inflationary complexity of thermal state

Tao Li and Lei-Hua Liu

Department of Physics, College of Physics, Mechanical and Electrical Engineering, Jishou University, Jishou 416000, China

E-mail: 2022700450@stu.jhu.edu.cn, liuleihua8899@hotmail.com

ABSTRACT: In this work, we systematically investigate the inflationary complexity of the two-mode squeezed state with thermal effect for the single field inflation, modified dispersion relation, and non-trivial sound speed with the method of closed system and open system, respectively. Since the various quantum gravitational framework could lead to this kind of modified dispersion relation and non-trivial sound speed, so that our analysis is valid for most inflationary models. (a). The numeric of Krylov complexity in the method of the closed system indicates that the evolution of Krylov complexity highly depends on the squeezed angle parameter once taking the thermal effect into account, which will decay into some very tiny values, but the Krylov complexity will always enhance without thermal effect. (b). The numeric of circuit complexity shows that the evolution is always increasing no matter whether there are thermal effects or not which is independent of the evolution of squeezed angle parameter. (c). By utilizing the method of open system, we first construct the wave function. Our investigations show the evolution of Krylov complexity will enhance upon some peaks factoring in the thermal effects and the Krylov complexity will always increase without thermal effect. (d). We also calculate the Krylov entropy in the method of closed system and open system, which indicates that the hotter the universe is, the more chaotic the universe becomes. Furthermore, our derivation for the Krylov complexity and Krylov entropy could nicely recover into the case of closed system under the weak dissipative approximation, which confirms the validity of construction for the wave function. Finally, our numeric of Lanczos coefficient shows that the non-trivial sound speed has minimal chaos compared to the other two cases.

Contents

1	Introduction	1
2	The thermal state	3
3	Krylov complexity and Lanczos algorithm with an approach of closed system	4
4	Three cases of inflationary models	6
4.1	Standard case	6
4.2	Non-trivial sound speed	7
4.3	The modified dispersion relation	8
5	Evolution of squeezed parameters $r_k(\eta)$ and $\phi_k(\eta)$	9
5.1	$r_k(\eta)$, $\phi_k(\eta)$ of standard case	9
5.2	$r_k(\eta)$, $\phi_k(\eta)$ of non-trivial sound speed	10
5.3	$r_k(\eta)$, $\phi_k(\eta)$ of modified dispersion relation	10
6	Krylov complexity with an approach of closed system	10
6.1	Krylov complexity of standard case	11
6.2	Krylov complexity of non-trivial sound speed	12
6.3	Krylov complexity of modified dispersion relation	13
7	Krylov Entropy	15
7.1	K-entropy of standard case	16
7.2	K-entropy of non-trivial sound speed	16
7.3	K-entropy of modified dispersion relation	17
8	Circuit complexity	18
8.1	Circuit complexity of standard case	21
8.2	Circuit complexity of non-trivial sound speed	22
8.3	Circuit complexity of modified dispersion relation	23
9	Krylov complexity with the approach of open system	24
9.1	Lanczos coefficient and dissipation coefficient	25
9.2	The wave function with open system's method	26
10	Evolution of Krylov complexity with approach of open system	28
10.1	Evolution of standard case	28
10.2	Evolution of non-trivial sound speed	29
10.3	Evolution of modified dispersion relation	30

11 K-entropy with the approach of open system	31
11.1 K-entropy of standard case	32
11.2 K-entropy of non-trivial sound speed	33
11.3 K-entropy of modified dispersion relation	33
12 Summary and outlook	34
A Wave function with thermal effect	37
B The equation of r_k and ϕ_k	39
C K-entropy with the approach of closed system	40
D Krylov complexity with approach of open system	41
E K-entropy with approach of open system	42

1 Introduction

The motivation for introducing the complexity is from [1], which stated that the boundary conformal field theory will reach the thermal equilibrium in a short time scale, and its corresponding bulk gravity will evolve to a certain state with a much longer time. To solve this problem, Refs. [2, 3] have proposed that the so-called complexity, where the evolution of spacetime is responded by the complexity, and the quantum entanglement produces the spacetime in light of holographic principle.

With the development of complexity in high energy physics, it is quite natural to investigate the complexity in quantum field theory (QFT) without the holographic principle. As for the computational complexity, it was defined as the minimal procedures for a certain task [4]. Although the definition of the complexity is still not unified, there are several methods for calculating the so-called circuit complexity. One is the so-called geometrical method pioneered by Nielson, *e.t.c* [5–7]. Another way is explicitly related to the "Fubini-Study" distance of information geometry [8]. Within these two methods, what they are investigating is the so-called circuit complexity dubbed as the minimal quantum operations from the reference state to the target state, especially for the first method. For the third method, we can define the Krylov complexity which is free of ambiguities compared with the previous two methods. Due to the uniqueness of Krylov complexity, we will compare the evolution between the Krylov complexity and circuit complexity so that one can obtain the differences and similarities. Ref. [9] proposed a universal operator growth. Once the quantum state is given, we can investigate the Krylov complexity, Lanczos coefficient, and Krylov entropy (K-entropy) in light of Lanczos algorithm [10]. For the connection between the Krylov complexity and circuit complexity, Ref. [11] has shown that the Krylov complexity is not compatible with circuit complexity. Whereas under certain conditions, the Krylov complexity will be proportional to the "Fubini-Study" distance.

In recent years, there has been significant progress in the development of complexity in high-energy physics. Circuit complexity can be obtained using the wave function method [12–14] and the covariance matrix method [15–20]. Although the definition of complexity is still in its preliminary stages, Ref. [12] has attempted to define it in QFT. These methods have also helped to relate complexity to a crucial aspect of the quantum chaos web of diagnostics [21–26]. Ref. [27] has systematically investigated the Krylov complexity using various polynomials referred to as the inner product. The concept of Krylov complexity can be applied into SKY model [28–30], generalized coherent state [31], Ising and Heisenberg models [32–34], conformal field theory [35, 36], topological phases of matter [37]. The chaos can be understood as the delocalization in Krylov space [38]. Based on the universal operator growth, Ref. [39] showed that the exponential growth of Krylov complexity can be observed in integrable systems with saddle-dominated scrambling. Then, Ref. [40] has verified all of the universal features of spread complexity within saddle dominated scrambling. The very recent developments of Krylov complexity can be found in Refs. [41–55].

The aim of this paper is to investigate the complexity of the inflationary period, including the circuit complexity and Krylov complexity. Prior research has been conducted in this direction [56–60]. Our previous research has shown that there is an oscillation of circuit complexity in inflation, which there is a similar trend after inflation [61–63]. However, Ref. [63] has shown that there is an irregular oscillation in inflation for the modified dispersion relation, which is common in many quantum gravitational frameworks. Most research has focused on the circuit complexity. However, several studies have investigated the Krylov complexity for the cosmological field. Ref. [64] investigated the Krylov complexity in inflation with various values of sound speed using a closed system approach. However, since the whole universe is an open system, Ref. [65] investigated the Krylov complexity in the method of open system, taking the wide validity of the modified dispersion relation for inflation into account. The findings revealed that the whole inflationary period is a strong dissipative system, and the total trend of Krylov complexity is increasing. The key point of [65] is constructing the wave function based on [66].

Both the closed and open systems utilize the two-mode squeezed state in constructing the wave function. However, to accurately demonstrate the realistic evolution of Krylov complexity, one must consider the thermal effects that occurred in the early universe. The high temperature during inflationary period led to the expansion of the universe and the generation of particles. Therefore, it is important to factor in these thermal effects. Ref. [67] has defined a thermalized Krylov complexity. As for the cosmological field, Ref. [68] has investigated the circuit complexity of the thermal state, where they found that the circuit complexity will decrease which is not the same with a pure two-mode squeezed state. From the hot nature of the universe, one can see that the investigation of the thermal squeezed state will be more dependable and practical compared with the pure two-mode squeezed state. Being armed with the thermal squeezed state, we expect that our analysis of complexity will be valid for the most inflationary models. Based on the universality, we will follow the [69] and [70] since string theory, Dirac-Born-Infeld (DBI), loop gravity and parity violation *e.t.c* will lead to these kinds of non-trivial sound speed [71–74] and

modified dispersion relation [75–80]. Of course, it will naturally include the standard single field inflation. Thus, we could see that our analysis will almost cover the whole inflationary models.

We organize the paper as follows. In Sec. 2, we will introduce the two-mode squeezed state. Then, Sec. 3 will give a brief introduction to the Lanczos algorithm with an approach of a closed system for the Krylov complexity. Sec. 4 will give three cases of inflationary models, including the standard case, modified dispersion relation, and non-trivial sound speed. Sec. 5 will show the numeric of ϕ_k and r_k for these three cases. Based on it, the numerical solutions of Krylov complexity will be given in Sec. 6. The Krylov entropy will be calculated in Sec. 7. For comparison, we will also calculate the circuit complexity in Sec. 8. In Sec. 9 and 10, we will show the Krylov complexity for these cases in the method of open system. For completeness, we will also give the detailed calculation of Krylov entropy in Sec. 11. Finally, the conclusion and outlook will be given in Sec. 12.

2 The thermal state

During inflation, the energy is very high characterized by the temperature. In this work, we aim to explore the complexity of the curvature perturbation during inflation. For better reflecting the real situation of complexity, the wave function with thermal effect is more dependable and practical compared to a pure two-mode squeezed state, which is defined in [81],

$$|\psi\rangle = \exp[\mathcal{K}(\hat{c}_k^\dagger \hat{c}_{-\vec{k}}^\dagger - \hat{c}_{\vec{k}} \hat{c}_{-\vec{k}})] |00\rangle_{\vec{k}, -\vec{k}} \quad (2.1)$$

where \mathcal{K} is related to the temperature and satisfies with $\cosh \mathcal{K} = \frac{1}{\sqrt{1-e^{-\frac{\omega}{T}}}}$, $\sinh \mathcal{K} = \frac{1}{\sqrt{e^{-\frac{\omega}{T}}-1}}$ (ω is the frequency of each mode), we will have the following values for the later investigations, $\mathcal{K} = (5, 10, 15, 19)$, the corresponding temperature $T = (5.1 \times 10^3 K, 1.1 \times 10^8 K, 2.4 \times 10^{12} K, 1.1 \times 10^{18} K)$.

In order to relate with the two-mode squeezed state, we will follow the notation of [82, 83] to define the following operator,

$$\hat{S}_k(\mathcal{K}, \frac{\pi}{2}) = \exp[\mathcal{K}(\hat{c}_k^\dagger \hat{c}_{-\vec{k}}^\dagger - \hat{c}_{\vec{k}} \hat{c}_{-\vec{k}})] \quad (2.2)$$

where we have used $\phi = \pi/2$. Being armed with this operator, we could define the two-mode squeezed state with thermal effect [84],

$$|\psi_T\rangle = \hat{S}_k(r_k, \phi_k) \hat{R}_k(\theta_k) \hat{S}_k(\mathcal{K}, \frac{\pi}{2}) |00\rangle_{\vec{k}, -\vec{k}} \quad (2.3)$$

where $\hat{R}_k(\theta_k)$ is the two-mode rotation operator and $\hat{S}_k(r_k, \phi_k)$ is the two-mode squeezed operator.

$$\hat{S}_k(r_k, \phi_k) = \exp[r_k(\eta)(e^{-2i\phi_k(\eta)} \hat{c}_{\vec{k}} \hat{c}_{-\vec{k}} - e^{2i\phi_k(\eta)} \hat{c}_k^\dagger \hat{c}_{-\vec{k}}^\dagger)] \quad (2.4)$$

$$\hat{R}_k(\theta_k) = \exp[-i\theta_k(\eta)(\hat{c}_{\vec{k}} \hat{c}_k^\dagger + \hat{c}_{-\vec{k}}^\dagger \hat{c}_{-\vec{k}})] \quad (2.5)$$

where $r_k(\eta)$ and $\phi_k(\eta)$ are the radial and angular parameters, respectively. The rotational parameter (2.5) only contribute the phase factor for the wave function, which will not impact the evolution, then we could obtain

$$|\psi_T\rangle = \hat{S}_k(r_k, \phi_k) \hat{R}_k(\theta_k) \hat{S}_k(\mathcal{K}, \frac{\pi}{2}) |00\rangle_{\vec{k}, -\vec{k}} \quad (2.6)$$

Put Eqs. (2.2), (2.4) and (2.5) into Eq. (2.6),

$$\begin{aligned} |\psi_T\rangle = & \exp[r_k(\eta)] (e^{-2i\phi_k(\eta)} \hat{c}_{\vec{k}} \hat{c}_{-\vec{k}} - e^{2i\phi_k(\eta)} \hat{c}_{\vec{k}}^\dagger \hat{c}_{-\vec{k}}^\dagger) \exp[-i\theta_k(\eta) (\hat{c}_{\vec{k}} \hat{c}_{\vec{k}}^\dagger + \hat{c}_{-\vec{k}}^\dagger \hat{c}_{-\vec{k}})] \\ & \cdot \exp[\mathcal{K} (\hat{c}_{\vec{k}}^\dagger \hat{c}_{-\vec{k}}^\dagger - \hat{c}_{\vec{k}} \hat{c}_{-\vec{k}})] |00\rangle_{\vec{k}, -\vec{k}} \end{aligned} \quad (2.7)$$

To find the wave function, we made the following transformation

$$\begin{cases} \frac{-e^{2i\phi_k} \sinh \beta}{\cosh \beta} = -e^{2i\phi_k} \tanh r_k \\ \frac{e^{2i\phi_k} \sinh \beta}{\cosh \beta} = e^{-2i\phi_k} \tanh r_k, \beta^2 = r_k^2 \end{cases} \quad (2.8)$$

Being armed with this transformation, we could obtain its resulting formula (detailed calculation as shown in appendix A),

$$|\psi_T\rangle = \frac{e^{-i\theta_k}}{\cosh r_k} \sum_{n=0}^{\infty} (\mathcal{K} - e^{2i\phi_k} \tanh r_k)^n |n; n\rangle_{\vec{k}, -\vec{k}} \quad (2.9)$$

This is one of our central results that will be utilized for investigating the Krylov complexity and its corresponding circuit complexity, but it is in the method of closed system. If we set $\theta_k = 0$ and $\mathcal{K} = 0$ since the latter investigation for Krylov complexity and circuit complexity which are all independent of θ_k , it will nicely recover into the standard two-mode squeezed state as $|\psi_T\rangle = \frac{1}{\cosh r_k} \sum_{n=0}^{\infty} (-1)^n e^{2in\phi_k} \tanh^n r_k |n; n\rangle_{\vec{k}, -\vec{k}}$.

In this section, we have introduced the two-mode squeezed state with thermal effect (2.9), which is of the temperature effects. Next, we will give the introduction of the Krylov complexity and Lanczos algorithm with the approach of closed system. Although [84] has defined the most general formalism of the two-mode squeezed state with thermal effects in terms of Lagrangian for the multi-scalar field, they did not derive the wave function after acting on the vacuum state. Our derivation is the first one for constructing the wave function after explicitly acting on the vacuum state.

3 Krylov complexity and Lanczos algorithm with an approach of closed system

In this section, we will introduce the Krylov complexity in the method of closed system. First, we need to define quantum mechanics in terms of Heisenberg operator $\mathcal{O}(t)$,

$$\partial_t \mathcal{O}(t) = i[H, \mathcal{O}(t)], \quad (3.1)$$

Its solution is

$$\mathcal{O}(t) = e^{iHt} \mathcal{O} e^{-iHt} \quad (3.2)$$

Furthermore, we could define the Liouvillian super-operator \mathcal{L}_X as $\mathcal{L}_X Y = [X, Y]$ (the same commutator with (3.1)). Under the Liouvillian super-operator, one can obtain $\mathcal{O}(t)$ as follows,

$$\mathcal{O}(t) = e^{i\mathcal{L}t}\mathcal{O} = \sum_{n=0}^{\infty} \frac{(it)^n}{n!} \mathcal{L}^n \mathcal{O}(0) = \sum_{n=0}^{\infty} \frac{(it)^n}{n!} \tilde{\mathcal{O}}_n \quad (3.3)$$

where $\mathcal{O}(t)$ can be dubbed as the wave function, using $\mathcal{L}^n \mathcal{O} = \tilde{\mathcal{O}}_n = [H, \tilde{\mathcal{O}}_{n-1}]$ to form the Hilbert space,

$$\mathcal{O} \equiv |\tilde{\mathcal{O}}\rangle, \mathcal{L}^1 \mathcal{O} \equiv |\tilde{\mathcal{O}}_1\rangle, \mathcal{L}^2 \mathcal{O} \equiv |\tilde{\mathcal{O}}_2\rangle, \mathcal{L}^3 \mathcal{O} \equiv |\tilde{\mathcal{O}}_3\rangle \dots \quad (3.4)$$

however, the basis is not orthogonal, consequently we could construct the orthogonal basis using the Lanczos algorithm, named by Krylov basis, where the first two terms are

$$\mathcal{O}_0 = |\tilde{\mathcal{O}}_0\rangle = \mathcal{O}, |\mathcal{O}_1\rangle = b_1^{-1} \mathcal{L}|\mathcal{O}_0\rangle, \quad (3.5)$$

where $b_1 = \sqrt{\langle \tilde{\mathcal{O}}_0 | \mathcal{L} | \tilde{\mathcal{O}}_0 \rangle}$ is the normalized vector, other orthogonal basis can be formed by the iterative relation,

$$|A_n\rangle = \mathcal{L}|\mathcal{O}_{n-1}\rangle - b_{n-1}|\mathcal{O}_{n-2}\rangle \quad (3.6)$$

with

$$|\mathcal{O}_n\rangle = b_n^{-1} |A_n\rangle, b_n = \sqrt{\langle A_n | A_n \rangle} \quad (3.7)$$

As $b_n = 0$, this iterative relation will stop and that will generate the finite orthogonal Krylov basis, where b_n is the so-called Lanczos coefficient. Thereafter, we could expand \mathcal{O} as follows

$$\mathcal{O}(t) = e^{i\mathcal{L}t}\mathcal{O} = \sum_{n=0}^{\infty} (i)^n \phi_n(t) |\mathcal{O}_n\rangle, \quad (3.8)$$

where ϕ_n is the real amplitude dubbed as the wave function, and $\sum_n |\phi_n|^2 = 1$. Through the Schrödinger equation, we can obtain

$$\partial_t \phi_n(t) = b_n \phi_{n-1} - b_{n-1} \phi_{n+1} \quad (3.9)$$

Afterwards, the Krylov complexity can be obtained from the following formula

$$K = \sum_n n |\phi_n|^2 \quad (3.10)$$

In addition, it can be inferred that the Lanczos coefficient is linearly bounded [9],

$$b_n \leq \alpha n + \gamma \quad (3.11)$$

where α and η are the parameters encoding various values in different models and the maximal value of b_n denotes the maximal chaos of the dynamical system. As for this maximal chaos, we could use the Lyapunov index γ to describe the chaotic growth of system as follows,

$$\gamma = 2\alpha. \quad (3.12)$$

Before investigating the complexity of two-mode squeezed state with thermal effect, we need to introduce three broad kinds of inflationary models nearly covering all of the inflationary models.

4 Three cases of inflationary models

In this section, we will provide a brief introduction to three cases of inflationary models. The first one is the single field inflation, which is commonly known as the standard case. The second one is the modified dispersion relation for inflation, which is applicable for loop gravitational inflation, Lorentz violation, string cosmology, and other similar models. Lastly, the non-trivial sound speed of inflation is another model that can be applied to many quantum gravitational frameworks. Therefore, our investigations are valid for most inflationary models.

In order to better understand the three types of inflationary models, it's important to have some fundamental knowledge about inflation. During inflation, the universe experienced an exponential expansion from 10^{-36} seconds to 10^{-32} seconds, increasing its volume by a factor of e^{60} . This expansion is characterized by the scale factor $a = \exp(Ht)$, where $H = \frac{\dot{a}}{a}$ (with \dot{a} being the derivative of a with respect to time) is the Hubble parameter which can be considered a constant for simplicity. Using $dt = ad\eta$ (η being the conformal time), we can calculate $\eta = \frac{-1}{aH}$ which will be useful in later investigations. Another important concept is the horizon exit. During inflation, the wavelength of particles is short, but still longer than the scale of the universe. As the universe expands, its size eventually becomes larger than the wavelength, known as the horizon exit. This has a significant impact on the temperature fluctuations observed via cosmic microwave background (CMB).

4.1 Standard case

In this paper, we will use the Friedman–Lemaître—Robertson Walker background metric,

$$ds^2 = a(\eta)^2(-d\eta^2 + d\vec{x}^2), \quad (4.1)$$

where $\vec{x} = (x, y, z)$ is the spatial vector and $a(\eta)$ is the scale factor in conformal time. Due to the re-enter of the horizon, this process can be characterized by the Hubble radius, thus the conformal time is more convenient comparing with physical time. Meanwhile, for defining the Mukhanov-Sasaki variable, the metric (4.1) can be rewritten by

$$ds^2 = a(\eta)^2 \left(-(1 + \psi(\eta, x))d\eta^2 + (1 - \psi(\eta, x))d\vec{x}^2 \right), \quad (4.2)$$

where $\psi(\eta, x)$ is the perturbation of metric, we can also define $\phi(x_\mu) = \phi_0(\eta) + \delta\phi(x_\mu)$ (ϕ is the inflaton). Once having these two perturbations, we can write the quadratic

perturbation can be written by,

$$S = \frac{1}{2} \int dt d^3x a^3 \frac{\dot{\phi}}{H^2} \left[\dot{\mathcal{R}} - \frac{1}{a} (\partial_i \mathcal{R})^2 \right], \quad (4.3)$$

where $H = \frac{\dot{a}}{a}$, $\mathcal{R} = \psi + \frac{H}{\dot{\phi}_0} \delta\phi$, $z = \sqrt{2\epsilon}a$, $\epsilon = -\frac{\dot{H}}{H^2} = 1 - \frac{H'}{H^2}$. Furthermore, we could write action (4.3) in terms of Mukhanov-Sasaki variable as follows,

$$S = \frac{1}{2} \int d\eta d^3x [v'^2 - (\partial_i v)^2 + \left(\frac{z'}{z}\right)^2 v^2 - 2v'v\frac{z'}{z}] \quad (4.4)$$

where $v = z\mathcal{R}$. Since we need the squeezed operator to act on the wave function, the Hamiltonian will be denoted in terms of creation and annihilation operators, respectively. In order to construct the Hamiltonian operator, we need to define the conjugate momentum

$$\pi(\eta, \vec{x}) = \frac{\delta L}{\delta v'(\eta, \vec{x})} = v' - \frac{z'}{z}v. \quad (4.5)$$

Then, we could construct the Hamiltonian via $H = \int d^3x d\eta (\pi v' - \mathcal{L})$,

$$H = \frac{1}{2} \int d^3x d\eta \left[\pi^2 + (\partial_i v)^2 + \frac{z'}{z}(\pi v + v\pi) \right]. \quad (4.6)$$

Using the Fourier decomposition,

$$\hat{v}(\eta, \vec{x}) = \int \frac{d^3k}{(2\pi)^{3/2}} \sqrt{\frac{1}{2k}} (\hat{c}_k^\dagger v_k^*(\eta) e^{-i\vec{k}\cdot\vec{x}} + \hat{c}_{-\vec{k}} v_{-\vec{k}} e^{i\vec{k}\cdot\vec{x}}), \quad (4.7)$$

$$\hat{\pi}(\eta, \vec{x}) = i \int \frac{d^3k}{(2\pi)^{3/2}} \sqrt{\frac{k}{2}} (\hat{c}_k^\dagger u_k^*(\eta) e^{-i\vec{k}\cdot\vec{x}} - \hat{c}_{-\vec{k}} u_{-\vec{k}} e^{i\vec{k}\cdot\vec{x}}). \quad (4.8)$$

Consequently, we could obtain the operator of Hamiltonian

$$\hat{H}_k = k(\hat{c}_{-\vec{k}}^\dagger \hat{c}_{-\vec{k}} + \hat{c}_{\vec{k}} \hat{c}_k^\dagger) - i\frac{z'}{z}(\hat{c}_k^\dagger \hat{c}_{-\vec{k}}^\dagger - \hat{c}_{\vec{k}} \hat{c}_{-\vec{k}}) \quad (4.9)$$

Based on the these concepts, we could introduce the non-trivial sound speed in inflation.

4.2 Non-trivial sound speed

The so-called non-trivial sound speed means (characterized by c_s^2) that the kinetic term is not canonical anymore, which will have some effects come via various quantum gravitational frameworks [85, 86]. By defining $z = \frac{\sqrt{2\epsilon}a}{c_s}$, the corresponding equation of motion (EOM) is

$$v_k'' + (c_s^2 k^2 - \frac{z''}{z})v_k = 0, \quad (4.10)$$

where we have transformed into the momentum space. One can see that the EOM (4.10) will nicely recover into the standard case as $c_s^2 = 1$. This non-trivial sound speed could appear in string theory [71, 72], Dirac-Born-Infeld (DBI) action [73]. From the perspective of effective field theory, we can obtain the non-trivial sound speed after integrating the heavy modes [74]. In this paper, we will focus on the mechanism of sound speed resonance (SSR)

[70], which it has many phenomenological implementations, the corresponding formula of c_s^2 is

$$c_s^2 = 1 - 2\xi[1 - \cos(k_*\tau)] \quad (4.11)$$

where ξ is the amplitude of oscillation and $k = nk_*$ is the frequency of oscillation that will lead to the production of primordial black-hole (PBH). Let us explain a little more about this SSR mechanism. By calculating its power spectrum, one could discover that the power spectrum will be enhanced by this kind of oscillation at $k = nk_*$ during small scales. Physically speaking, it will generate the PBH that could account for dark matter nearly covering all of the mass range. Thus, it could lead to the rich phenomenological implementations dubbed as the motivation for choosing this kind of SSR. According to EOM (4.10), one can easily obtain its corresponding action

$$S = \frac{1}{2} \int d\eta d^3x [v'^2 - c_s^2(\partial_i v)^2 + (\frac{z'}{z})^2 v^2 - 2v'v\frac{z'}{z}]. \quad (4.12)$$

Following the same procedure with Sec. 4.1, we can obtain the Hamiltonian in terms of conjugate momentum,

$$H = \frac{1}{2} \int d^3x [\pi^2 + c_s^2(\partial_i^2 v) + \frac{z'}{z}(\pi v + v\pi)]. \quad (4.13)$$

Being armed with the Fourier decomposition (4.7) (4.8), Hamiltonian operator in momentum space can become as follows,

$$\hat{H}_k = \frac{k}{2}(c_s^2 + 1)(\hat{c}_{-k}^\dagger \hat{c}_{-k} + \hat{c}_k \hat{c}_k^\dagger) + (\frac{k}{2}(c_s^2 - 1) + i\frac{z'}{z})\hat{c}_k^\dagger \hat{c}_{-k}^\dagger + (\frac{k}{2}(c_s^2 - 1) - i\frac{z'}{z})\hat{c}_k \hat{c}_{-k} \quad (4.14)$$

The next case we consider is the modified dispersion relation in inflation.

4.3 The modified dispersion relation

The modified dispersion in inflation was proposed by [69], where many quantum gravitational frameworks could lead to this kind of modified dispersion relation. Its corresponding action can read as

$$S = \frac{1}{2} \int d\eta d^3x \left[v'^2 - f_{ph}^2(\partial_i v)^2 + (\frac{z'}{z})^2 v^2 - 2\frac{z'}{z}v'v \right], \quad (4.15)$$

with

$$\begin{cases} \text{if } (k_{ph}) > M; f = (\frac{k_{ph}}{M})^\alpha \\ \text{if } (k_{ph}) \leq M; f = 1 \end{cases} \quad (4.16)$$

where $k_{ph} = \frac{k}{a}$ denotes the physical wave number. Various values of α will determine different kinds of quantum gravitational models, it can summarize as follows:

(a). The standard dispersion relation corresponds to $\alpha = 0$ is also the standard inflationary model [87], which belongs to the *IR* regime

(b). As $0 < \alpha < 2$, it also belongs to the *UV* regime.

(c). As $\alpha = 2$, it is a special kind of Horva-Lifshitz cosmology [88, 89].

(d). As $\alpha > 2$, it also belongs to the UV regime.

Once having the action (4.15), one can following the similar procedure to construct the quantum Hamiltonian operator as follows,

$$\hat{H}_k = \frac{k}{2}(f^2 + 1)(\hat{c}_{-k}^\dagger \hat{c}_{-k} + \hat{c}_k \hat{c}_k^\dagger) + \left(\frac{k}{2}(f^2 - 1) + i\frac{z'}{z}\right)\hat{c}_k^\dagger \hat{c}_{-k}^\dagger + \left(\frac{k}{2}(f^2 - 1) - i\frac{z'}{z}\right)\hat{c}_k \hat{c}_{-k}. \quad (4.17)$$

In Sec. 4, we have presented three cases of inflationary models. The first case is the standard one, also known as single-field inflation. The second case is inflation with a modified dispersion relation, which various quantum gravitational frameworks could lead to this kind of modified dispersion relation. The last one is inflation with a non-trivial sound speed, which has rich phenomenological implications. Our discussion has helped us realize that we have covered most inflationary models. The second issue is that the Hamiltonian (4.9), (4.14), (4.17) are explicitly proved to be Hermitian. Although these three Hamiltonian are all Hermitian, but the wave function for the closed system's method and open system's method is different. In the latter investigations, we will show the details.

5 Evolution of squeezed parameters $r_k(\eta)$ and $\phi_k(\eta)$

According to our previous research [61, 63, 65], we find that the complexity needs the evolution of $r_k(\eta)$ and $\phi_k(\eta)$ in a method of closed system. In this section, we will show the calculation of $r_k(\eta)$ and $\phi_k(\eta)$ in three cases. Our starting wave function is Eq. (2.9), and it satisfies with the Schrodinger equation,

$$i\frac{d}{d\eta}|\psi_T\rangle = \hat{H}_k|\psi_T\rangle, \quad (5.1)$$

where the Hamiltonian operator corresponds (4.9), (4.14), (4.17), respectively. Next, we will show their equation of evolution case by case.

5.1 $r_k(\eta)$, $\phi_k(\eta)$ of standard case

By using the Hamiltonian in Eq. (4.9), we can obtain the evolution equations of $r_k(\eta)$ and $\phi_k(\eta)$ whose detailed calculations are performed in Appendix B.

$$\begin{aligned} r'_k &= \frac{a'}{a}\mathcal{K}\coth r_k - \frac{a'}{a}\cos(2\phi_k) \\ \phi'_k &= k\mathcal{K}\cos(2\phi_k)\coth r_k - k + \frac{a'}{a}\sin(2\phi_k)[\coth(2r_k) - \frac{1}{2}\mathcal{K}^2\coth r_k] \end{aligned} \quad (5.2)$$

where we have approximated ϵ to be a constant since the background of inflation can be dubbed as a quasi-De Sitter spacetime, thus we could obtain $\frac{z'}{z} = \frac{a'}{a}$ with $z = a\sqrt{2\epsilon}$. If

there were no thermal effects, Eq. (5.2) will recover into

$$\begin{aligned} r'_k &= -\frac{a'}{a} \cos(2\phi_k), \\ \phi'_k &= -k + \frac{a'}{a} \sin(2\phi_k) \coth(2r_k), \end{aligned} \quad (5.3)$$

which is consistent with [60], in which Ref. [90] was the first one who derived the Eq. (5.3).

5.2 $r_k(\eta)$, $\phi_k(\eta)$ of non-trivial sound speed

Following the similar calculation, we could obtain the $r_k(\eta)$ and $\phi_k(\eta)$ as follows,

$$r'_k = \mathcal{K} \frac{a'}{a} \coth r_k + \frac{k}{2} (c_s^2 - 1) \sin(2\phi_k) - \frac{a'}{a} \cos(2\phi_k), \quad (5.4)$$

$$\begin{aligned} \phi'_k &= -\frac{k}{2} (c_s^2 + 1) - \frac{k\mathcal{K}}{2} (c_s^2 - 1) + \sin(2\phi_k) \left[\frac{a'}{a} \coth(2r_k) - \frac{a'}{2a} \mathcal{K}^2 \coth r_k \right] \\ &\quad + \cos(2\phi_k) \left[\frac{k\mathcal{K}}{2} (c_s^2 + 1) \coth r_k + \frac{k}{4} \mathcal{K}^2 (c_s^2 - 1) \coth r_k + \frac{k}{2} (c_s^2 - 1) \coth(2r_k) \right]. \end{aligned} \quad (5.5)$$

When $\mathcal{K} = 0$ (without thermal effect) and $c_s^2 = 1$ (normal speed of sound), the evolution of the squeezed parameters r_k and ϕ_k in the above equation perfectly returns to Eq. (5.3).

5.3 $r_k(\eta)$, $\phi_k(\eta)$ of modified dispersion relation

In this case, we could obtain

$$r'_k = \mathcal{K} \frac{a'}{a} \coth r_k + \frac{k}{2} (f^2 - 1) \sin(2\phi_k) - \frac{a'}{a} \cos(2\phi_k), \quad (5.6)$$

$$\begin{aligned} \phi'_k &= -\frac{k}{2} (f^2 + 1) - \frac{k\mathcal{K}}{2} (f^2 - 1) + \sin(2\phi_k) \left[\frac{a'}{a} \coth(2r_k) - \frac{a'}{2a} \mathcal{K}^2 \coth r_k \right] \\ &\quad + \cos(2\phi_k) \left[\frac{k\mathcal{K}}{2} (f^2 + 1) \coth r_k + \frac{k}{4} \mathcal{K}^2 (f^2 - 1) \coth r_k + \frac{k}{2} (f^2 - 1) \coth(2r_k) \right]. \end{aligned} \quad (5.7)$$

One could discover that (5.6) and (5.7) is quite similar with (5.4) and (5.5), the only difference comes via c_s^2 and f^2 , which both of them play the same role from the perspective of mathematics. As $f^2 = 1$, it will nicely recover into the standard case.

In Sec. 5, we have shown the analytical equation of evolution of ϕ_k and r_k in three cases. Being armed these ones, we could use them to investigate the Krylov complexity with closed system's method.

6 Krylov complexity with an approach of closed system

In this section, we will use the wave function (2.9) for exploring the Krylov complexity in closed system's method. In light of (3.10), we could find the corresponding operator wave function as follows,

$$\phi_n = \frac{e^{-i\theta_k}}{\cosh r_k} (\mathcal{K} - e^{2i\phi_k} \tanh r_k)^n. \quad (6.1)$$

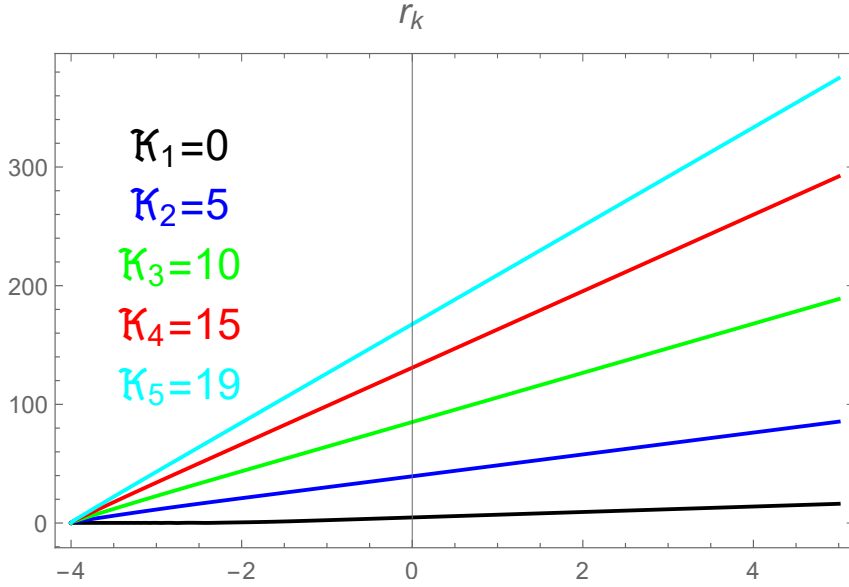


Figure 1. The numerical solution of $r_k(\eta)$ in terms of $\log_{10} a$ for the standard case, which we have set $\mathcal{K}_1 = 0$, $\mathcal{K}_2 = 5$, $\mathcal{K}_3 = 10$, $\mathcal{K}_4 = 15$, and $\mathcal{K}_5 = 19$. Our plot adopts $H = 1$, and $k = 0.01$.

Also according to the definition of Krylov complexity, we could explicitly obtain

$$K = \frac{1}{\cosh^2 r_k} \frac{\mathcal{K}^2 - 2\mathcal{K} \tanh r_k \cos(2\phi_k) + \tanh^2 r_k}{[1 - (\mathcal{K}^2 - 2\mathcal{K} \tanh r_k \cos(2\phi_k) + \tanh^2 r_k)]^2}. \quad (6.2)$$

It is worth noting that the value of θ_k does not affect the Krylov complexity. The Krylov complexity is influenced by r_k and ϕ_k together, which is unlike the Krylov complexity without thermal effects, as shown in [65]. Through a simple algebraic calculation, we can obtain that $K = \sinh^2 r_k$ with $\mathcal{K} = 0$, which confirms that the wave function in equation (2.9) is correct. This formula of Krylov complexity is valid for the thermal state and could be a criterion for assessing the accuracy of the wave function in the weak dissipative approximation.

6.1 Krylov complexity of standard case

In Section 5.1, we already obtained the evolution of the squeezed parameters $r_k(\eta)$ and $\phi_k(\eta)$ as shown in Eq. (5.2), which is very difficult for solving. In order to numerically solve this equation, we transform Eq. (5.2) into

$$\begin{aligned} \frac{dr_k}{dy} &= \ln 10 \mathcal{K} \coth r_k - \ln 10 \cos(2\phi_k) \\ \frac{d\phi_k}{dy} &= \frac{\ln 10}{10^y H} k \mathcal{K} \cos(2\phi_k) \coth r_k - \frac{\ln 10}{10^y H} k + \ln 10 \sin(2\phi_k) [\coth(2r_k) - \frac{1}{2} \mathcal{K}^2 \coth r_k] \end{aligned} \quad (6.3)$$

where we have denoted $y = \log_{10} a$.

Once it is ready, we will be able to obtain the numerical values of $\phi_k(\eta)$ and $r_k(\eta)$ for the standard case, as presented in Figures 1 and 2. These figures indicate that the value

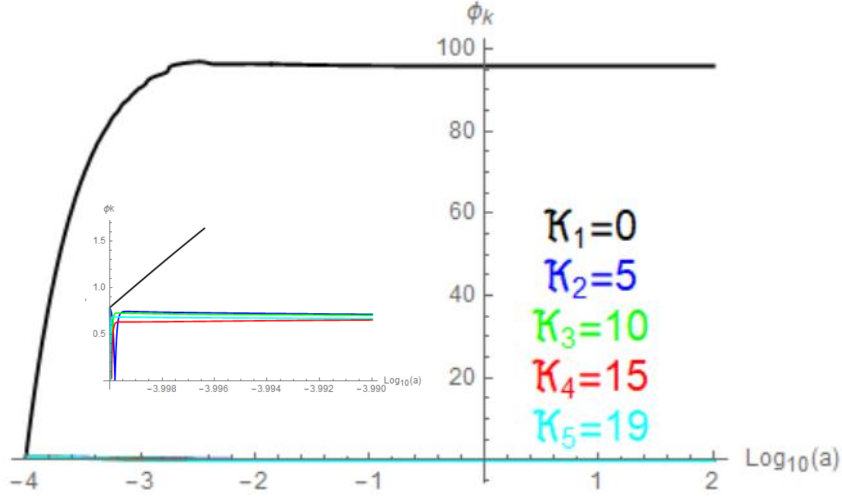


Figure 2. The numerical solution of $\phi_k(\eta)$ in terms of $\log_{10} a$ for the standard case, which we have set $\mathcal{K}_1 = 0$, $\mathcal{K}_2 = 5$, $\mathcal{K}_3 = 10$, $\mathcal{K}_4 = 15$, and $\mathcal{K}_5 = 19$. Our plots adopt $H = 1$, and $k = 0.01$.

of r_k increases as \mathcal{K} increases, whereas the trend of ϕ_k is the opposite. Taking the thermal effects into account, the order of ϕ_k is approximately 0.8. We will observe that this type of evolution of ϕ_k will have a significant impact on its corresponding Krylov complexity, which is distinct from our previous research [63]. In our previous research, the values of ϕ_k without thermal effects had almost no effect on the circuit complexity

Fig. 3 clearly indicates that the Krylov complexity will increase as we move towards larger scales, and there is an initial oscillation that is consistent with the findings in [65]. However, when thermal effects are taken into account, the Krylov complexity will decay to some constant values, when we increase the values of \mathcal{K} . By analyzing Figs. 1 and 2 along with Fig. 3, it is evident that the evolution of Krylov complexity with thermal effect is mainly determined by ϕ_k . On the other hand, when thermal effects are negligible, the evolution of Krylov complexity is mainly determined by r_k .

6.2 Krylov complexity of non-trivial sound speed

By introducing the variable $y = \log_{10} a$, Eqs. (5.4) and (5.5) could become as follows:

$$\frac{dr_k}{dy} = \ln 10 \mathcal{K} \coth r_k + \frac{\ln 10}{10^y H} \frac{k}{2} (c_s^2 - 1) \sin(2\phi_k) - \ln 10 \cos(2\phi_k) \quad (6.4)$$

$$\begin{aligned} \frac{d\phi_k}{dy} = & -\frac{\ln 10}{10^y H} \frac{k}{2} (c_s^2 + 1) - \frac{\ln 10}{10^y H} \frac{k\mathcal{K}}{2} (c_s^2 - 1) + \sin(2\phi_k) \left[\ln 10 \coth(2r_k) - \frac{1}{2} \frac{\ln 10}{10^y H} \mathcal{K}^2 \coth r_k \right] \\ & + \frac{\ln 10}{10^y H} \cos(2\phi_k) \left[\frac{k\mathcal{K}}{2} (c_s^2 + 1) \coth r_k + \frac{k}{4} \mathcal{K}^2 (c_s^2 - 1) \coth r_k + \frac{k}{2} (c_s^2 - 1) \coth(2r_k) \right] \end{aligned} \quad (6.5)$$

Being armed with these two equations, we could utilize their numeric to simulate the evolution of Krylov complexity in the non-trivial sound speed.

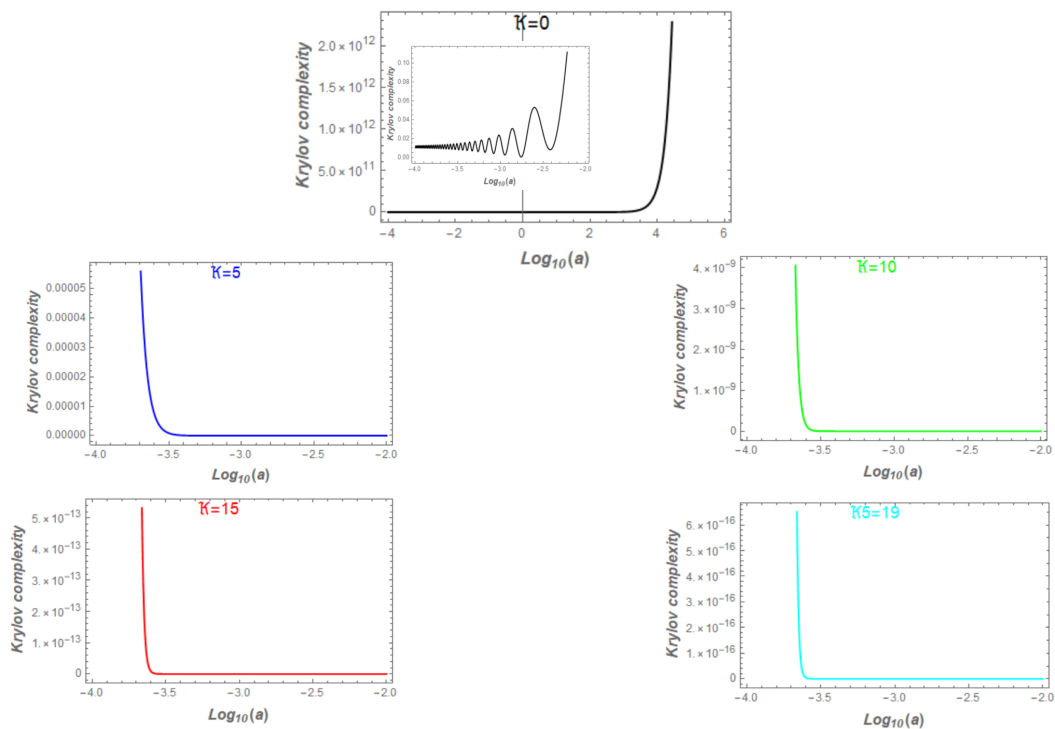


Figure 3. The numerical solutions of Krylov complexity in terms of $\log_{10} a$ for the standard case, where we have set $\mathcal{K} = 0, 5, 10, 15, 19$. Our plots adopt $H = 1$, and $k = 0.01$.

Fig. 4 displays the Krylov complexity of non-trivial sound speed varying with ξ and \mathcal{K} . In this figure, various values of ξ are determined by observational constraints via [70]. The trend of evolution indicates that the Krylov complexity will decrease almost to vanishing with thermal effect, and the larger value of ξ will speed up this process. Our numerical analysis shows that the evolution of ϕ_k with thermal effect will lead to the decreasing trend of Krylov complexity during inflation, which is consistent with the discussions in Sec. 6.1. On the other hand, without thermal effects, we discovered that the total trend of Krylov complexity always increases during the entire inflationary period, and the larger value of ξ will speed up this issue, where the evolution of complexity is mainly determined by r_k and not by ϕ_k . Additionally, we find that the larger value of ξ , which denotes the more oscillation of sound speed, leads to more chaos in the dynamical system. Physically speaking, the process of PBH generation will cause more chaos as $\mathcal{K} = 0$.

6.3 Krylov complexity of modified dispersion relation

Following the similar procedure, we could rewrite the evolution of r_k and ϕ_k in terms of $\log_{10} a$,

$$\frac{dr_k}{dy} = \ln 10 \mathcal{K} \coth r_k + \frac{\ln 10}{10^y H} \frac{k}{2} (f^2 - 1) \sin(2\phi_k) - \ln 10 \cos(2\phi_k) \quad (6.6)$$

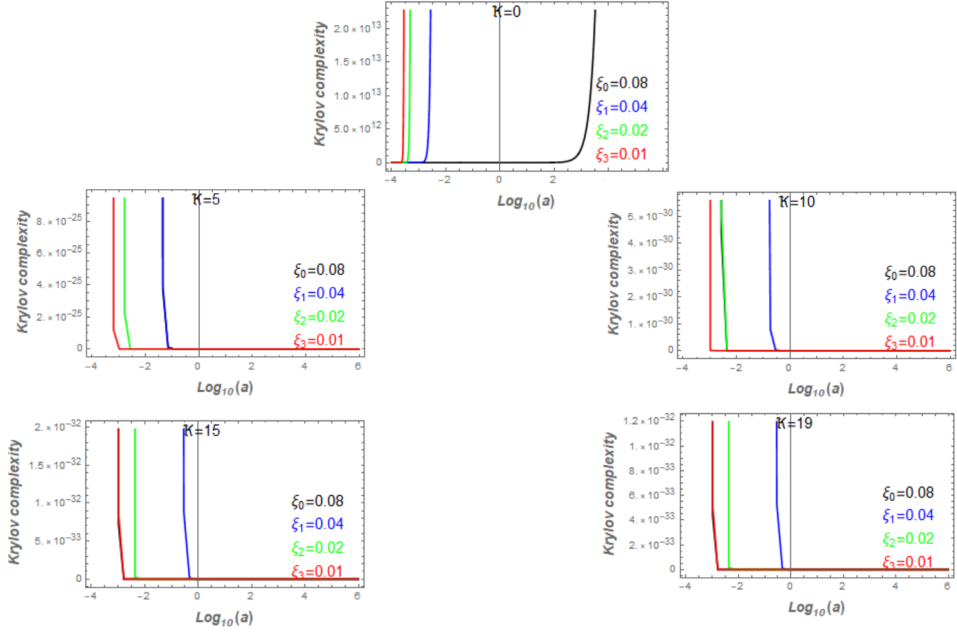


Figure 4. The numerical solutions of Krylov complexity in terms of $\log_{10} a$ with $\mathcal{K}_1 = 0$ for the non-trivial sound speed, $\mathcal{K}_2 = 5$, $\mathcal{K}_3 = 10$, $\mathcal{K}_4 = 15$ and $\mathcal{K}_5 = 19$. And we set $\xi = 0.01$, $\xi = 0.02$, $\xi = 0.04$ and $\xi = 0.08$. Our plots adopt $H = 1$, and $k = 0.01$.

$$\begin{aligned}
\frac{d\phi_k}{dy} = & -\frac{\ln 10}{10^y H} \frac{k}{2} (f^2 + 1) - \frac{\ln 10}{10^y H} \frac{k\mathcal{K}}{2} (f^2 - 1) + \sin(2\phi_k) [\ln 10 \coth(2r_k) - \frac{1}{2} \frac{\ln 10}{10^y H} \mathcal{K}^2 \coth r_k] \\
& + \frac{\ln 10}{10^y H} \cos(2\phi_k) \left[\frac{k\mathcal{K}}{2} (f^2 + 1) \coth r_k + \frac{k}{4} \mathcal{K}^2 (f^2 - 1) \coth r_k + \frac{k}{2} (f^2 - 1) \coth(2r_k) \right]
\end{aligned} \tag{6.7}$$

We will also implement their numeric to analyze the evolution of Krylov complexity for the modified dispersion relation in inflation.

Fig. 5 illustrates the evolution of Krylov complexity with respect to varying values of α and \mathcal{K} for the modified dispersion relation. The values of α were obtained from [63]. Since the formulas (6.7) and (6.6) are almost identical to (5.4) and (5.5), the overall trend seen in Fig. 5 is the same as that in Fig. 4. When thermal effects are taken into account, the Krylov complexity decreases until it reaches a very small value, and larger values of f^2 lead to a faster decay of Krylov complexity as determined by ϕ_k rather than r_k . For $\mathcal{K} = 0$, the trend of Krylov complexity is always increasing, and larger values of α (i.e., larger values of f^2) lead to a faster growth of Krylov complexity.

In Sec. 6, we have already investigated the evolution of Krylov complexity for three cases, including the standard case, non-trivial sound speed, and modified dispersion relation. Our study reveals that the Krylov complexity of these three cases decreases once taking the thermal effects into account since the evolution of Krylov complexity is mainly determined by ϕ_k , not r_k . As for $\mathcal{K} = 0$, the Krylov complexity of these three cases always grows in an inflationary period, in which the more values of temperature (denoted by \mathcal{K}),

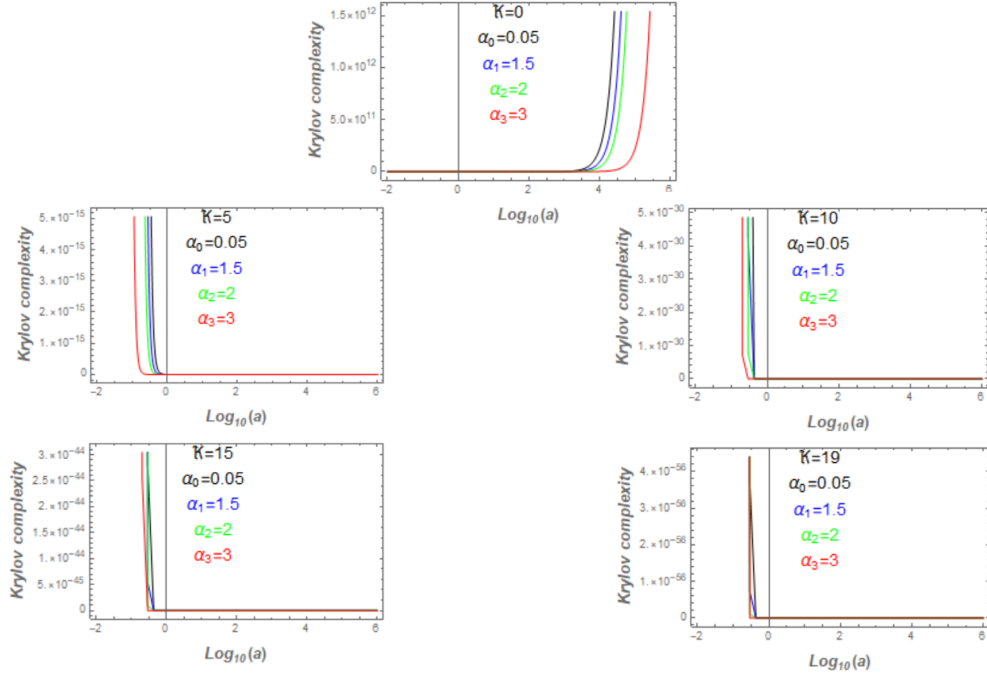


Figure 5. The numerical solutions of Krylov complexity in terms of $\log_{10} a$ with $\mathcal{K}_1 = 0$, $\mathcal{K}_2 = 5$, $\mathcal{K}_3 = 10$, $\mathcal{K}_4 = 15$ and $\mathcal{K}_5 = 19$ for the modified dispersion relation. And we set $\alpha = 0.00$, $\alpha = 1.5$, $\alpha = 2$ and $\alpha = 30$. Our plots adopt $H = 1$, and $k_{ph}/M = 1.5$.

non-trivial sound speed (presented by ξ) and modified dispersion relation (via f^2), the more growth of their corresponding Krylov complexity. Thus, we can conclude that the evolution of ϕ_k with thermal effect mainly determines the Krylov complexity which has not been found before.

7 Krylov Entropy

In a quantum system, entropy is defined to measure the disorder of a system. In the framework of Krylov complexity, the Krylov entropy (K-entropy) could test the level of disorder of curvature perturbation in our case. Similarly, with the definition of von Neumann entropy, we could also define the K-entropy following from [26],

$$S_K = - \sum_{n=0}^{\infty} |\phi_n|^2 \ln |\phi_n|^2, \quad (7.1)$$

where ϕ_n is Eq. (6.1). Then, the expression of K-entropy can be obtained by calculation as follows (detailed calculation can be found in Appendix C),

$$\begin{aligned}
S_K &= - \sum_{n=0}^{\infty} |\phi_n|^2 \ln |\phi_n|^2 \\
&= - \sum_{n=0}^{\infty} \frac{x^n}{\cosh^2 r_k} (n \ln x - 2 \ln \cosh r_k) \\
&= \frac{2 \ln \cosh r_k - x \ln [x \cosh^2 r_k]}{[\cosh r_k (1-x)]^2}
\end{aligned} \tag{7.2}$$

where $x = \mathcal{K}^2 - 2\mathcal{K} \tanh r_k \cos 2\phi_k + \tanh^2 r_k$, it is obvious that the evolution of K-entropy is related to the squeezed parameters r_k and ϕ_k . When $\mathcal{K} = 0$, that is $x = \tanh^2 r_k$, without thermal effect, K-entropy can perfectly return to the form in Ref. [64],

$$S_K = \cosh^2 r_k \ln \cosh^2 r_k - \sinh^2 r_k \ln \sinh^2 r_k. \tag{7.3}$$

Thus, this calculation confirms that the wave function with thermal effect (2.9) is correct. Subsequently, we could investigate the K-entropy in three cases: the standard case, the non-trivial sound speed and the modified dispersion relation.

7.1 K-entropy of standard case

Sec. 6.1 provides the numerical values of ϕ_k and r_k for the standard case. Using these values and K-entropy equation (7.2), we can plot the K-entropy figure for the standard case. Figure 6 displays the evolution of K-entropy for the standard case, which reveals that K-entropy increases with temperature (represented by \mathcal{K}). This matches with our physical intuition that the hotter the universe, the more chaotic it becomes. Interestingly, K-entropy exhibits oscillatory behavior when the temperature is zero, which means that the level of the K-entropy is not stable not like the case with thermal effect.

7.2 K-entropy of non-trivial sound speed

Being armed with Sec. 6.2 and K-entropy (7.2), we could obtain the evolution of K-entropy for the non-trivial sound speed as shown in Fig. 7. Here, we need to emphasize that the plot with $\mathcal{K} = 19$ is almost identical with $\mathcal{K} = 15$ which is not listed here. When the thermal effects are taken into account, one can see that the same trend with the standard case, the universe is more chaotic as enhancing the temperature (denoted by \mathcal{K}), and meanwhile we almost cannot distinguish between the SSR and the standard case. As for the case without thermal effects, one could see that there is irregular oscillation before the horizon exits ($\log_{10} a = -2$), and the K-entropy will grow after the horizon exits. Since the horizon exit will transit the curvature perturbation from the quantum level to the classic level, one could see that the universe will be more chaotic when it becomes classical in the case of $\mathcal{K} = 0$, and the large value of non-trivial sound speed will also enhance the K-entropy a little comparing with standard case, physically speaking, the formation of PBH will lead to this phenomenon.

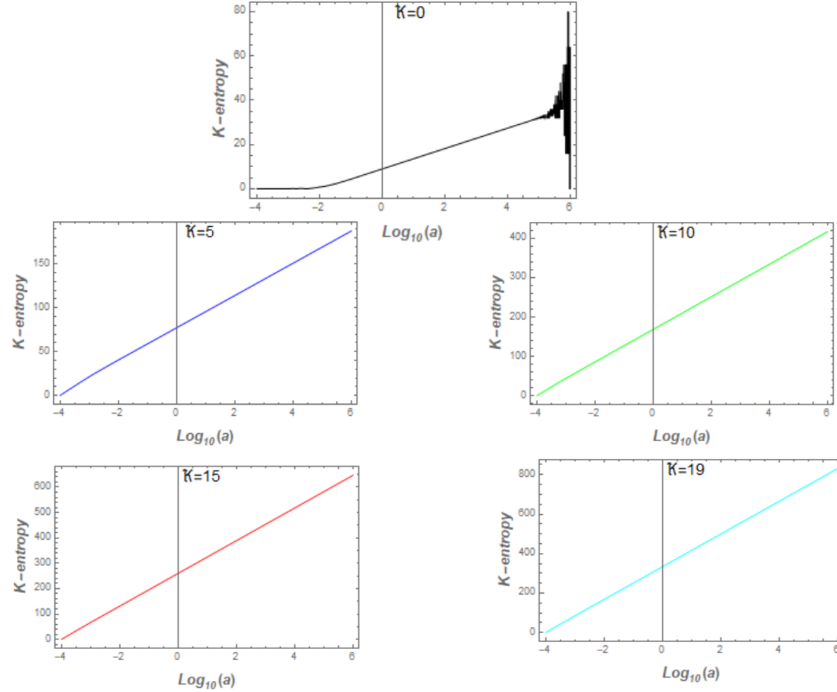


Figure 6. The numerical solutions of K-entropy in terms of $\log_{10} a$ with $\mathcal{K}_1 = 0$, $\mathcal{K}_2 = 5$, $\mathcal{K}_3 = 10$, $\mathcal{K}_4 = 15$ and $\mathcal{K}_5 = 19$ for the standard case. Our plots adopt $H = 1$, and $k = 0.01$. The horizon exits occur at $\log_{10} a = -2$.

7.3 K-entropy of modified dispersion relation

Comparing with Figs. 6, 7, Fig. 8 indicates more colorful evolution of K-entropy. First, let's discuss the K-entropy without thermal effects, one can see that there is oscillation before the horizon exits, and the K-entropy will continue growing after that. Meanwhile, we could see that larger values of f^2 determined by α will lead to the faster oscillation of the K-entropy, which means the quantum gravitational framework could lead to this kind of oscillatory behavior. Second, we will come to the discussion for the case with thermal effect. The most essential trend is that the K-entropy will be enhanced by improving the temperature determined by \mathcal{K} . Meanwhile, one can see that the larger values of α will lead to the bigger values of K-entropy in each panel, which means that the various quantum gravitational frameworks will also lead to this kind of phenomenon. More deeply speaking, the case of modified dispersion relation compared with the single field inflation will lead to more chaos under the same conditions.

In Sec. 7, we already have investigated the K-entropy in three cases. Due to the nature of entropy, we have found that the hotter the universe, the more chaotic the universe, which is valid for all three cases. The interesting place is that the K-entropy will show the oscillation as $\mathcal{K} = 0$, which is also valid for these three cases, and the horizon exit will

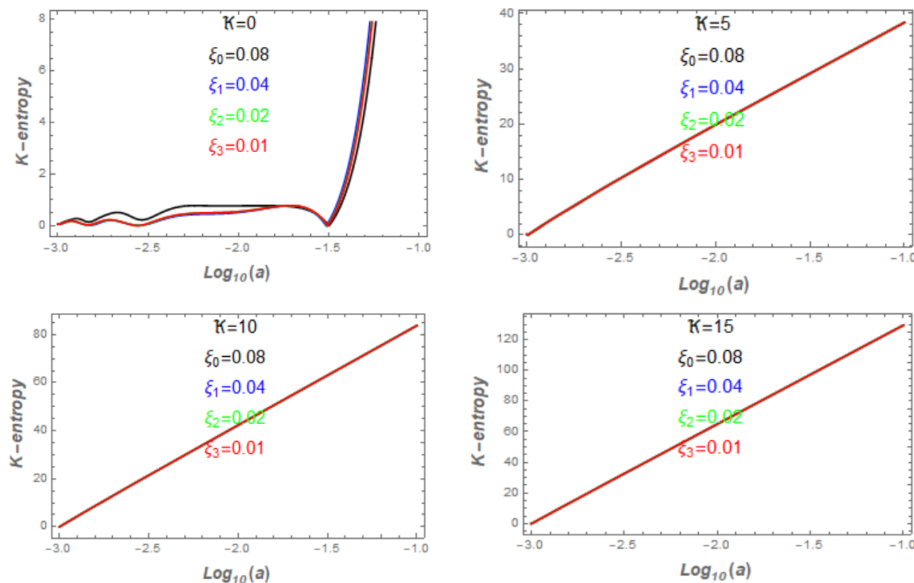


Figure 7. The numerical solutions of K-entropy in terms of $\log_{10} a$ with $\mathcal{K}_1 = 0$, $\mathcal{K}_2 = 5$, $\mathcal{K}_3 = 10$ and $\mathcal{K}_4 = 15$ for the non-trivial sound speed. And we set $\xi = 0.08$, $\xi = 0.04$, $\xi = 0.02$ and $\xi = 0.01$. Our plots adopt $H = 1$, and $k = 0.01$. The horizon exits occur at $\log_{10} a = -2$.

lead to the K-entropy growth, which means the decoherence may impact the evolution of K-entropy left for the future work.

8 Circuit complexity

We already investigated the Krylov complexity for thermal state with the approach of a closed system. There is another way of evaluating the complexity called the circuit complexity, which is related to the choice of the parameter manifold. In this section, we will use the geometrical method for investigating the circuit complexity [5, 7], where we could compare the with the method of Krylov complexity and obtain their differences and similarities. First, we need a reference state $|\psi^R\rangle$ at $\eta = 0$, then we could relate to a target state at $\eta = 1$ via

$$|\psi^T\rangle_{\eta=1} = U(\eta = 1) |\psi^R\rangle_{\eta=0}, \quad (8.1)$$

where η parameterizes the path of Hilbert space and $U(\eta)$ is a path-ordered exponential of a Hamiltonian operator

$$U(\eta) = \overleftarrow{\mathcal{P}} \exp \left(-i \int_0^\eta ds H(s) \right), \quad (8.2)$$

where $\overleftarrow{\mathcal{P}}$ is the path ordering from right to left, and $H(s)$ is formed by a basis of Hermitian operators M_I base, which are the generators for elementary logic gates

$$H(s) = Y(s)^I M_I \quad (8.3)$$

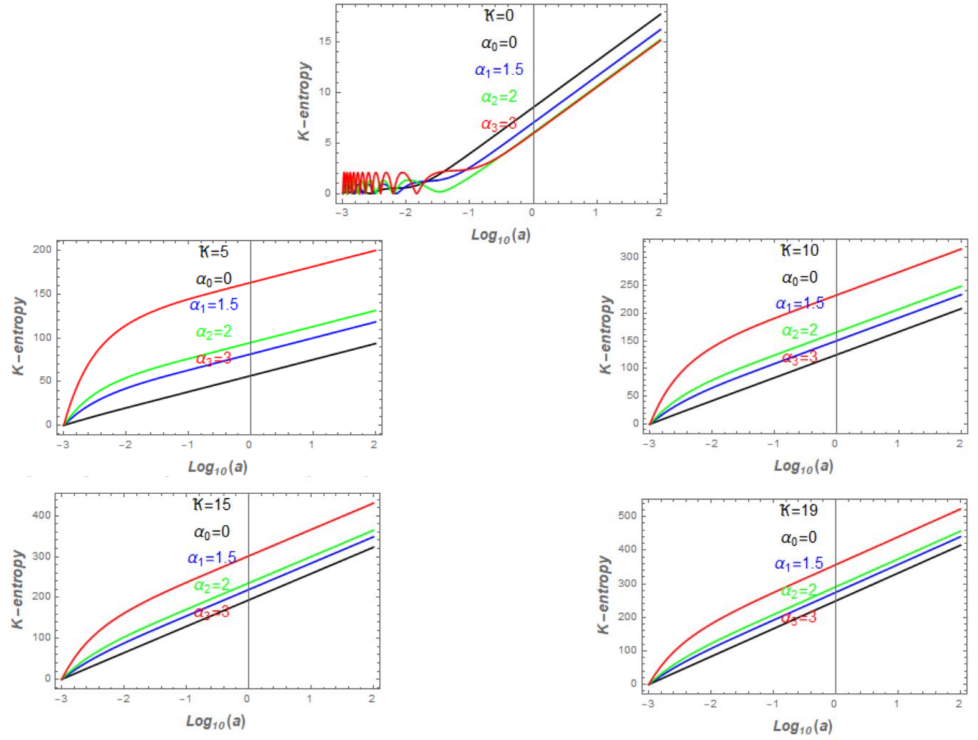


Figure 8. The numerical solutions of K-entropy in terms of $\log_{10} a$ with $\mathcal{K}_1 = 0$, $\mathcal{K}_2 = 5$, $\mathcal{K}_3 = 10$, $\mathcal{K}_4 = 15$ and $\mathcal{K}_5 = 19$ for the modified dispersion relation. And we set $\alpha = 0.00$, $\alpha = 1.5$, $\alpha = 2$ and $\alpha = 30$. Our plots adopt $H = 1$, and $k_{ph}/M = 1.5$. The horizon exits occur at $\log_{10} a = -2$.

where $Y(s)^I$ is defined as the control function that determines which gate will be switched on or switched off, and $Y(s)^I$ satisfies the Schrödinger equation

$$\frac{dU}{ds} = -iY(s)^I M_I U(s) \quad (8.4)$$

To define the circuit complexity, we introduce the function to associated with circuit complexity

$$C(U) = \int_0^1 \mathcal{F}(U, \dot{U}) d\eta. \quad (8.5)$$

The circuit complexity can be obtained by minimizing the cost function (8.5). Therefore, we can find the geodesic line between the reference state and target state. Here, we first focus on the quadratic cost function,

$$\mathcal{F}(U, Y) = \sqrt{\sum_l (Y^I)^2}. \quad (8.6)$$

In this work, the target state is a two-mode wave function , we can obtain its formula from ,

$$\begin{aligned}\Psi_{sq}(q_{\vec{k}}, q_{-\vec{k}}) &= \sum_{n=0}^{\infty} (-1)^n \frac{\tanh^n r_k}{\cosh^n r_k} \langle q_{\vec{k}}; q_{-\vec{k}} | n; n \rangle_{\vec{k}, -\vec{k}} \\ &= \frac{\exp[A(r_k, \phi_k) \cdot (q_{\vec{k}}^2 + q_{-\vec{k}}^2) - B(r_k, \phi_k) q_{\vec{k}} q_{-\vec{k}}]}{\cosh r_k \sqrt{\pi} \sqrt{1 - e^{-4i\phi_k} \tanh^2 r_k}},\end{aligned}\quad (8.7)$$

where $A(r_k, \phi_k)$ and $B(r_k, \phi_k)$ are

$$A(r_k, \phi_k) = \frac{k}{2} \left(\frac{e^{-4i\phi_k} \tanh^2 r_k + 1}{e^{-4i\phi_k} \tanh^2 r_k - 1} \right) \quad (8.8)$$

$$B(r_k, \phi_k) = \frac{k}{2} \left(\frac{e^{-2i\phi_k} \tanh^2 r_k}{e^{-4i\phi_k} \tanh^2 r_k - 1} \right) \quad (8.9)$$

Defining the vector space $(q_{\vec{k}}, q_{-\vec{k}})$, Eq. (8.7) can be rewritten by the diagonal matrix

$$\begin{aligned}\Psi_{sq}(q_{\vec{k}}, q_{-\vec{k}}) &= \frac{\exp[-\frac{1}{2} \tilde{M}^{ab} q_a q_b]}{\cosh r_k \sqrt{\pi} \sqrt{1 - e^{-4i\phi_k} \tanh^2 r_k}} \\ \tilde{M} &= \begin{pmatrix} \Omega_{\vec{k}'} & 0 \\ 0 & \Omega_{-\vec{k}'} \end{pmatrix} = \begin{pmatrix} -2A + B & 0 \\ 0 & -2A - B \end{pmatrix}\end{aligned}\quad (8.10)$$

Meanwhile, we consider the vacuum state as the reference state, it can be obtained following the standard procedure,

$$\begin{aligned}\Psi_{00}(q_{\vec{k}}, q_{-\vec{k}}) &= \langle q_{\vec{k}}; q_{-\vec{k}} | 0; 0 \rangle_{\vec{k}, -\vec{k}} \\ &= \frac{\exp[-\frac{1}{2} (\omega_{\vec{k}} q_{\vec{k}}^2 + \omega_{-\vec{k}} q_{-\vec{k}}^2)]}{\pi^{1/2}} \\ &= \frac{\exp[-\frac{1}{2} \tilde{M}^{ab} q_a q_b]}{\pi^{1/2}} \\ \tilde{M} &= \begin{pmatrix} \Omega_{\vec{k}'} & 0 \\ 0 & \Omega_{-\vec{k}'} \end{pmatrix},\end{aligned}\quad (8.11)$$

where (8.11) has the same structure as the target wave function (8.10), where both of them have the Gaussian distribution. Thus, the unitarity operator (8.2) will not change the structure of wave functions. Furthermore, we can relate reference state (8.11) to target state (8.10) via (8.2) as follows,

$$\Psi_{\eta}(q_{\vec{k}}, q_{-\vec{k}}) = \tilde{U}(\eta) \Psi_{00}(q_{\vec{k}}, q_{-\vec{k}}) \tilde{U}^{\dagger}(\eta), \quad (8.12)$$

$$\Psi_{\eta=0}(q_{\vec{k}}, q_{-\vec{k}}) = \Psi_{00}(q_{\vec{k}}, q_{-\vec{k}}), \quad (8.13)$$

$$\Psi_{\eta=1}(q_{\vec{k}}, q_{-\vec{k}}) = \Psi_{sq}(q_{\vec{k}}, q_{-\vec{k}}), \quad (8.14)$$

where $U(\eta)$ is a $GL(2, C)$ unitary matrix which gives the shortest line between the reference state and target state. As Ref. [12] discussed, $U(\eta)$ can be rewritten by

$$\tilde{U}(\eta) = \exp\left[\sum_{k=1}^2 Y^k(\eta) M_k^{\text{diag}}\right], \quad (8.15)$$

where M_k^{diag} denotes two generators of $GL(2, C)$ as showing

$$M_1^{\text{diag}} = \begin{pmatrix} 1 & 0 \\ 0 & 0 \end{pmatrix}, M_2^{\text{diag}} = \begin{pmatrix} 0 & 0 \\ 0 & 1 \end{pmatrix} \quad (8.16)$$

As for $Y_I(\eta)$, it can be constructed via [91]

$$Y_I(\eta) = Y_I(\eta = 1) \cdot \eta + Y_I(\eta = 0) \quad (8.17)$$

From the boundary conditions of (8.13) and (8.14), we could obtain,

$$\text{Im}(Y^{1,2})|_{\eta=0} = \text{Re}(Y^I)|_{\eta=0} = 0, \quad (8.18)$$

$$\text{Im}(Y^{1,2})|_{\eta=1} = \frac{1}{2} \ln \frac{|\Omega_{\vec{k}, -\vec{k}}|}{\omega_{\vec{k}, -\vec{k}}}, \quad (8.19)$$

$$\text{Re}(Y^{1,2})|_{\eta=1} = \frac{1}{2} \arctan \frac{\text{Im}(\Omega_{\vec{k}, -\vec{k}})}{\text{Re}(\omega_{\vec{k}, -\vec{k}})}. \quad (8.20)$$

In light of these conditions, the circuit complexity is evaluated as the geodesic line of parametric manifold

$$C(\tilde{U}) = \int_0^1 d\eta \sqrt{G_{IJ} \dot{Y}^I(\eta) \dot{Y}^J(\eta)^*}, \quad (8.21)$$

where G_{IJ} is the induced metric for the group manifold. As [12] shown, the induced metric G_{IJ} could have an arbitrary structure for the group manifold. In our case, the group structure is $SL(2, C)$ that will lead to the flat geometry, namely $G_{IJ} = \delta_{IJ}$. Consequently, the final formula of circuit complexity is obtained as follows,

$$C(k) = \frac{1}{2} \left[\left(\ln \frac{|\Omega_{\vec{k}}|}{\omega_{\vec{k}}} \right)^2 + \left(\arctan \frac{\text{Im}(\Omega_{\vec{k}})}{\text{Re}(\omega_{\vec{k}})} \right)^2 \right. \\ \left. + \left(\ln \frac{|\Omega_{-\vec{k}}|}{\omega_{-\vec{k}}} \right)^2 + \left(\arctan \frac{\text{Im}(\Omega_{-\vec{k}})}{\text{Re}(\omega_{-\vec{k}})} \right)^2 \right]. \quad (8.22)$$

The information of various models is encoded in (8.8) and (8.9). The final formula of circuit complexity (8.22) will be implemented in three cases as mentioned in the previous section.

8.1 Circuit complexity of standard case

Combining the circuit complexity formula (8.22) with Eq. (5.2), we can determine the evolution of circuit complexity for the standard case. Fig. 9 clearly depicts the evolution of circuit complexity. The main feature of Fig. 9 is that the total trend of circuit complexity is

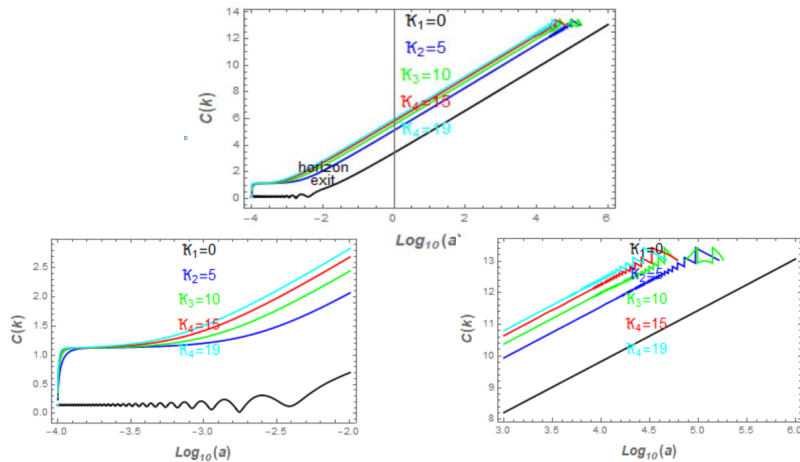


Figure 9. The numerical solutions of circuit complexity $C(k)$ in terms of $\log_{10} a$ with $\mathcal{K}_1 = 0$, $\mathcal{K}_2 = 5$, $\mathcal{K}_3 = 10$, $\mathcal{K}_4 = 15$ and $\mathcal{K}_5 = 19$ for the standard case. Our plots adopt $H = 1$, and $k = 0.01$. The horizon exits occur at $\log_{10} a = -2$. The below two panels showing the very beginning (-4.0 to -2.0) and the end (3.0 to 6.0) of the first panel.

always increasing, compared to the Krylov complexity whose trend decreases as \mathcal{K} is non-vanishing as shown in Fig. 3, regardless of whether the circuit complexity has thermal effects or not. However, the higher the temperature, the faster the growth of circuit complexity.

More precisely, we observe that the circuit complexity grows rapidly right from the beginning of the universe and then almost linearly with thermal effect. After the horizon exits, the circuit complexity with thermal effect shows irregular oscillations, as mentioned in [23]. The scrambling time, which marks the point where complexity begins to increase, is shorter for circuit complexity with thermal effect than the circuit complexity without thermal effects. On the other hand, the Lyapunov index can be dubbed as the slope of complexity when complexity becomes linear as shown, which denotes the chaotic nature of the system, is almost identical for both cases. This means that the universe was more chaotic in the early stages of its existence and its chaos remained more or less the same after the horizon exits, regardless of whether there were thermal effects or not.

8.2 Circuit complexity of non-trivial sound speed

Together with Eq. (8.22) and Eq. (5.5), Fig. 10 shows the plot of circuit complexity for the non-trivial sound speed. The plot indicates that the overall trend of circuit complexity always increases, regardless of whether there are thermal effects or not. The irregular oscillation of circuit complexity can be divided into two parts: one before the horizon exits and another after. In the first plot of Fig. 10, we observe that there is only an

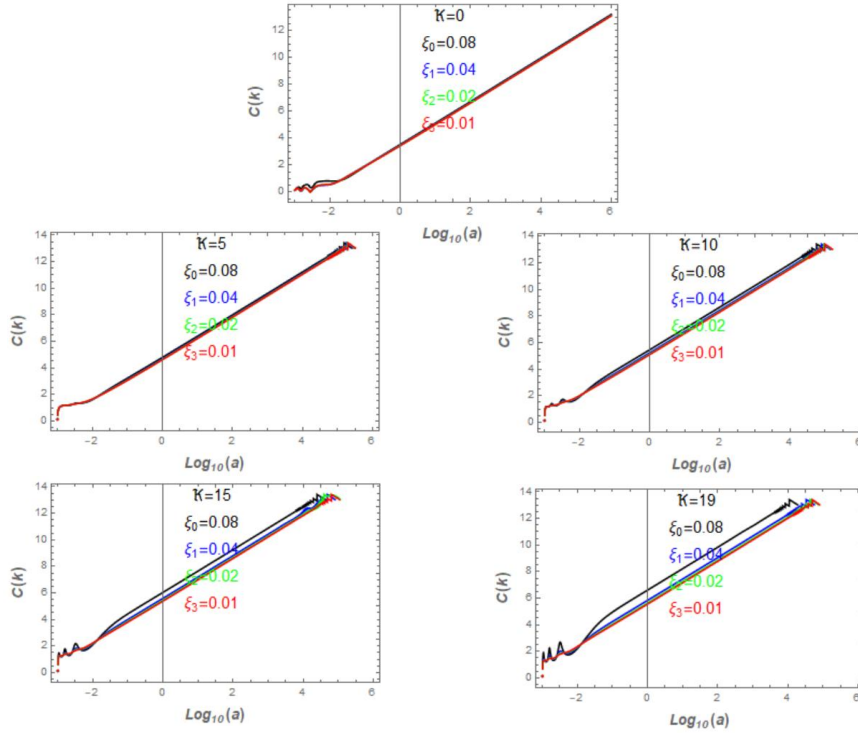


Figure 10. The numerical solutions of circuit complexity $C(k)$ in terms of $\log_{10} a$ with $\mathcal{K}_1 = 0$, $\mathcal{K}_2 = 5$, $\mathcal{K}_3 = 10$, $\mathcal{K}_4 = 15$ and $\mathcal{K}_5 = 19$ for the non-trivial sound speed. And we set $\xi = 0.08$, $\xi = 0.04$, $\xi = 0.02$ and $\xi = 0.01$. Our plots adopt $H = 1$, and $k = 0.01$. The horizon exits occur at $\log_{10} a = -2$.

oscillation of circuit complexity, and as the values of ξ increases, the oscillation of circuit complexity before the horizon exits becomes more pronounced. Thus, we conclude that PBH formation leads to this kind of oscillation before the horizon exits. When thermal effects are taken into account, we observe a second oscillation after the horizon exits. Our numerical analysis also reveals that higher temperatures lead to more oscillations of circuit complexity. Regarding the scrambling time and Lyapunov index, we find that it is almost impossible to distinguish between each plot of Fig. 10.

8.3 Circuit complexity of modified dispersion relation

Following Eq. (8.22), Eq. (6.6) and Eq. (6.7), we can get the plot of circuit complexity for the modified dispersion relation. Fig. 11 clearly shows the evolution of circuit complexity for the modified dispersion relation, which also shows more color evolution comparing with the previous cases. First, the total trend of circuit complexity is always increasing that includes the thermals effects or without thermal effects. Second, let's analyze the evolution of circuit complexity plot by plot. For the first plot, we can see that there are also two oscillations for the circuit complexity, the first one appears before the horizon exits, the second one occurs after that, where it indicates that the first oscillation will be more pronounced as $\alpha > 1$ and the other cases are very hard for distinguishing.

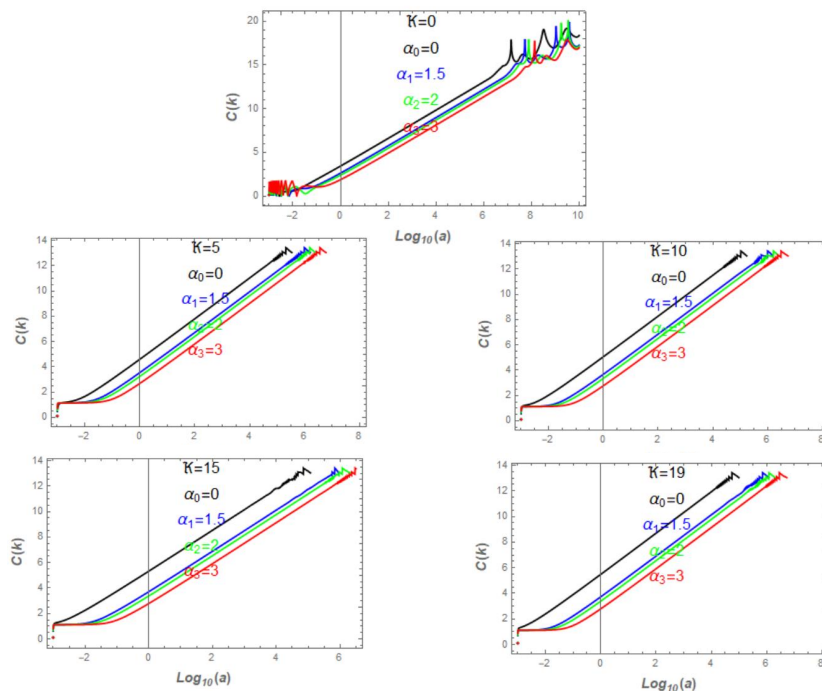


Figure 11. The numerical solutions of circuit complexity $C(k)$ in terms of $\log_{10} a$ with $\mathcal{K}_1 = 0$, $\mathcal{K}_2 = 5$, $\mathcal{K}_3 = 10$, $\mathcal{K}_4 = 15$ and $\mathcal{K}_5 = 19$ for the modified dispersion relation. And we set $\alpha = 0.00$, $\alpha = 1.5$, $\alpha = 2$ and $\alpha = 30$. Our plots adopt $H = 1$, and $k_{ph}/M = 1.5$. The horizon exits occur at $\log_{10} a = -2$.

The trend with thermal effect is quite similar, one can see that the temperature almost will not impact the evolution of circuit complexity. The only difference is that the scrambling time with $\alpha > 1$ is longer than the standard case ($\alpha = 0$) and the Lyapunov index of all is also quite similar, but when comparing with the case without thermal effects, one could see that the Lyapunov index of thermal effects is larger that is consistent with the reality. Physically speaking, the higher the temperature, the more chaotic of the very universe.

In Sec. 8, we have investigated the circuit complexity of three cases. Comparing with the Krylov complexity in Sec. 6, the total trend of circuit complexity is always increasing from the entire inflationary period, which is not so relevant to the evolution of ϕ_k but it is related to r_k . Meanwhile, our numeric also reveals that the Lyapunov index will be larger as enhancing the temperature in the case of non-trivial sound speed and modified dispersion relation, which means that the hotter the universe, the more chaotic the universe.

9 Krylov complexity with the approach of open system

In the previous analysis, we investigated the Krylov complexity in a method of closed system. According to [92, 93], it shows that our universe is an open system, and Ref. [65] has indicated that inflation is a strong dissipative system. Thus, the method of open

system for dealing with Krylov complexity is more dependable and realistic. In this section, we will utilize the method of open system to calculate the Lanczos coefficient, Lyapunov index, Krylov complexity.

9.1 Lanczos coefficient and dissipation coefficient

In this section, we will follow the method of [66] to investigate. First, the general operator in Heisenberg's picture to denote as follows,

$$\mathcal{O}(\eta) = e^{i\mathcal{L}_o\eta}, \quad (9.1)$$

where the Lindbladian \mathcal{L}_o represents the Hamiltonian in our paper, and it acts on the Krylov basis so as to obtain,

$$\mathcal{L}_o|\mathcal{O}_n\rangle = -ic_n|\mathcal{O}_n\rangle + b_{n+1}|\mathcal{O}_{n+1}\rangle + b_n|\mathcal{O}_{n-1}\rangle, \quad (9.2)$$

where c_n encodes the information of the open system and b_n is the Lanczos coefficient and Eq. (9.2) was first defined by [94]. The expression of Lindbladian \mathcal{L}_o in open system is as follows

$$\mathcal{L}_o = \mathcal{H}_o = \mathcal{H}_{close} + \mathcal{H}_{open}. \quad (9.3)$$

In our paper, we already have three Hamiltonian (Lindbladian) as shown in Eqs. (4.9), (4.14) and (4.17), corresponding the standard case, the non-trivial sound speed and the modified dispersion relation, respectively. In light of [65], these three Hamiltonian can be divided into two parts: the open part

$$\mathcal{H}_{open} = \begin{cases} k(\hat{c}_{-k}^\dagger \hat{c}_{-k} + \hat{c}_{-k} \hat{c}_{-k}^\dagger) \\ \frac{k}{2}(f^2 + 1)(\hat{c}_{-k}^\dagger \hat{c}_{-k} + \hat{c}_{-k} \hat{c}_{-k}^\dagger) \\ \frac{k}{2}(c_s^2 + 1)(\hat{c}_{-k}^\dagger \hat{c}_{-k} + \hat{c}_{-k} \hat{c}_{-k}^\dagger) \end{cases} \quad (9.4)$$

and the closed part

$$\mathcal{H}_{close} = \begin{cases} -i\frac{z'}{z}(\hat{c}_{-k}^\dagger \hat{c}_{-k}^\dagger - \hat{c}_{-k} \hat{c}_{-k}) \\ (\frac{k}{2}(f^2 - 1) + i\frac{z'}{z})\hat{c}_{-k}^\dagger \hat{c}_{-k}^\dagger + (\frac{k}{2}(f^2 - 1) - i\frac{z'}{z})\hat{c}_{-k} \hat{c}_{-k} \\ (\frac{k}{2}(c_s^2 - 1) + i\frac{z'}{z})\hat{c}_{-k}^\dagger \hat{c}_{-k}^\dagger + (\frac{k}{2}(c_s^2 - 1) - i\frac{z'}{z})\hat{c}_{-k} \hat{c}_{-k} \end{cases} \quad (9.5)$$

where $|\mathcal{O}_n\rangle = |n_{\vec{k}}; n_{-\vec{k}}\rangle$. In order to test accuracy of decomposition of Hamiltonian, one can use the open part of the standard case to plug into Eq. (9.2), one can straightforwardly obtain $c_n = i(2n + 1)k$. Here, we just list the resulting formulas of c_n and b_n for three cases:

$$c_n = \begin{cases} i(2n + 1)k \\ i(2n + 1)\frac{k}{2}(f^2 + 1) \\ i(2n + 1)\frac{k}{2}(c_s^2 + 1) \end{cases}, |b_n| = \begin{cases} n\frac{a'}{a} \\ n\sqrt{(\frac{k}{2}(f^2 - 1))^2 + (\frac{a'}{a})^2} \\ n\sqrt{(\frac{k}{2}(c_s^2 - 1))^2 + (\frac{a'}{a})^2} \end{cases} \quad (9.6)$$

The two quantities c_n and b_n in Eq. (9.6) are determined by Hamiltonian and there is no any thermal effects for them, and c_n encodes the information of dissipative coefficient, b_n measures the operator growth of one system. Also following the [66], we can find

$$b_n^2 = |1 - \mu_1^2|n(n - 1 + \beta), c_n = i\mu_2(2n + \beta), \quad (9.7)$$

where μ_2 plays a role of dissipative coefficient. Combining Eqs. (9.6) and (9.7), we define two parameters μ_1 and μ_2 as follows,

$$|1 - \mu_1|^2 = \begin{cases} \left(\frac{a'}{a}\right)^2 \\ \left(\frac{k}{2}(f^2 - 1)\right)^2 + \left(\frac{a'}{a}\right)^2 \\ \left(\frac{k}{2}(c_s^2 - 1)\right)^2 + \left(\frac{a'}{a}\right)^2 \end{cases}, \mu_2 = \begin{cases} k \\ \frac{k}{2}(f^2 + 1) \\ \frac{k}{2}(c_s^2 + 1) \end{cases} \quad (9.8)$$

where $\beta = 1$ in our case. Here, we will give a little more about b_n . Ref. [9] has proposed that the Lanczos coefficient will be satisfied with the following relation in the thermal limit,

$$b_n \leq \alpha n + \eta, \quad (9.9)$$

where α and η encodes the information of the system, when $b_n = \alpha n + \eta$ that means the system will reach the maximal chaos, we could find that $\eta = 0$ in our work and α is encoded in Eq. (9.6). Meanwhile we can find that three cases what we consider are perfectly matching $b_n \propto n$ which leads to the maximal chaos of inflation via [66], then the Lyapunov index λ will have relation

$$\lambda = 2\alpha, \quad (9.10)$$

where we can find a simple relation $b_n = 2\alpha$ as $n = 2$, the Lanczos coefficient represents the chaotic feature of the system. Consequently, we only plot b_n as a manifestation for illustrating the chaos and operator growth.

Fig. 12 clearly shows that the evolution of $b_n = \frac{1}{2}\lambda$ occurs at $n = 1$, where the background will dramatically impact the evolution of b_n presented by $\log_{10} a$. The first plot in Fig. 12 displays that the Lanczos coefficient is almost zero before the horizon exits, but after that, it starts to grow. A similar trend can be observed in the other two cases, but in the case of non-trivial sound speed, there will be oscillation before the horizon exits. Larger values of ξ will lead to larger oscillations of b_n . It is important to note that the order of b_n is higher for the standard case and modified dispersion relation when compared to the case of non-trivial sound speed. This means that single-field inflation and various quantum gravitational frameworks will result in the same level of chaos for inflation, but the formation of PBH will not lead to this order of chaos. Therefore, the chaos of inflation is mainly determined by the theoretical framework itself, rather than the formation of PBH.

9.2 The wave function with open system's method

Before the construction of the wave function, we will first discuss the validity of the method of [9], whose analysis is based on the asymptotic behaviour of $b_n^{(1)}$ (Lanczos coefficient),

$$b_n^{(1)} = \alpha n + \gamma, \quad (9.11)$$

where we discovered that the Lanczos coefficient in our case is consistent with the assumption of a valid b_n for infinite, non-integrable, many-body systems, as shown in Eq. (9.6). With this method, we were able to define two parameters, as shown in Eq. (9.7), which encode information about various models, as shown in Eq. (9.8). The advantage of our method is that it is valid for more realistic models, including various quantum gravitational

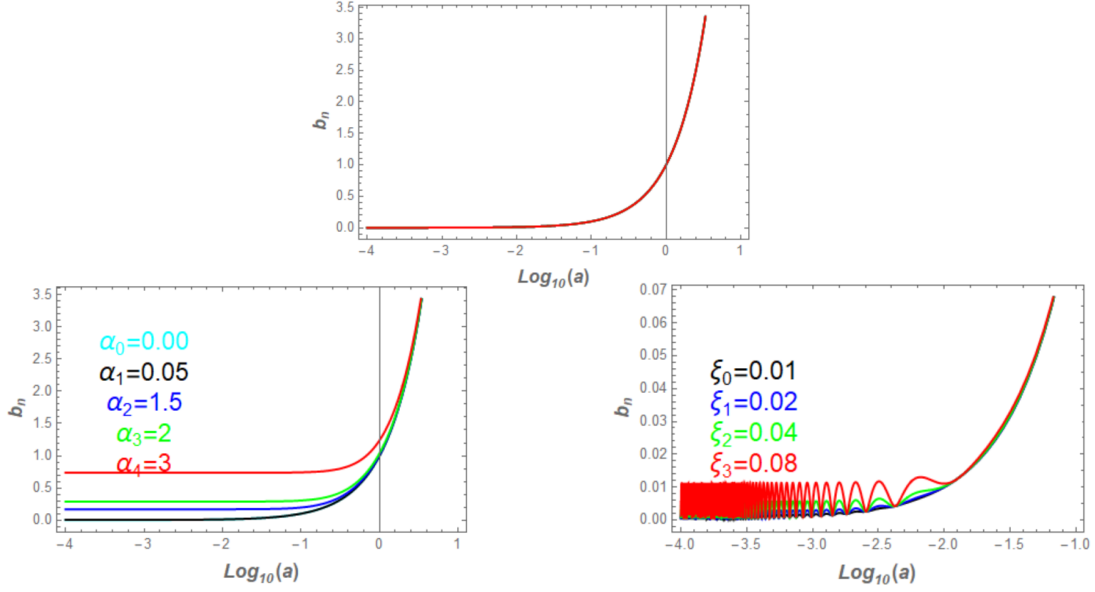


Figure 12. The numerical solutions of $b_n = \frac{1}{2}\lambda$ as $n = 1$ in terms of $\log_{10} a$. Our plots adopt $H = 1$, $k = 0.01$ and $k_{ph}/M = 1.5$. The horizon exits occur at $\log_{10} a = -2$.

frameworks, whereas the original method of [9] only focuses on one parameter corresponding to $\mu_1 = \mu_2 = \mu$ in our case, where μ takes some constant values. Ref. [65] extends the original method by constructing the wave function with the approach of an open system,

$$\phi_n = \frac{\text{sech } \eta}{1 + \mu_2 \tanh \eta} |1 - \mu_1^2|^{\frac{n}{2}} \left(\frac{\tanh \eta}{1 + \mu_2 \tanh \eta} \right)^n, \quad (9.12)$$

where we have tested its validity by calculating Krylov complexity and K-entropy under the weak dissipative approximation, which could nicely recover into the case with the method of closed system. Being armed this construction (9.12), we similarly construct as follows

$$\phi_n = \frac{\text{sech } \eta}{1 + \mu_2 \tanh \eta} |1 - \mu_1^2|^{\frac{n}{2}} \left(\mathcal{K} - \frac{\tanh \eta}{1 + \mu_2 \tanh \eta} \right)^n \quad (9.13)$$

Then, we will proceed with this wave function for the Krylov complexity under (3.10), one can explicitly obtain the Krylov complexity

$$K = \frac{\text{sech}^2 \eta |1 - \mu_1^2| [\mathcal{K}^2 + \tanh \eta (2\mathcal{K}^2 \mu_2 - 2\mathcal{K}) + \tanh^2 \eta (\mathcal{K} \mu_2 - 1)^2]}{\left\{ (1 + \mu_2 \tanh \eta)^2 - |1 - \mu_1^2| [\mathcal{K}^2 + \tanh \eta (2\mathcal{K}^2 \mu_2 - 2\mathcal{K}) + \tanh^2 \eta (\mathcal{K} \mu_2 - 1)^2] \right\}^2}. \quad (9.14)$$

We analyze the Krylov complexity in two limits. The first one is without thermal effects, namely $\mathcal{K} = 0$, Eq. (9.14) will return into the Krylov complexity with the open system's method,

$$K = \frac{\text{sech}^2 \eta |1 - \mu_1^2| \tanh^2 \eta}{[1 + 2\mu_2 \tanh \eta + (\mu_2^2 - |1 - \mu_1^2|) \tanh^2 \eta]^2}, \quad (9.15)$$

which it is consistent with [65]. As for the second case, when the $\mu_1 \ll 1$ and $\mu_2 \ll 1$, we could obtain the leading order of Eq. (9.14) as follows

$$K = \frac{1}{\cosh^2 \eta} \frac{\mathcal{K}^2 - 2\mathcal{K} \tanh \eta + \tanh^2 \eta}{[1 - (\mathcal{K}^2 - 2\mathcal{K} \tanh \eta + \tanh^2 \eta)]^2} + \mathcal{O}^n(\mu_2), \quad (9.16)$$

which is also consistent with Eq. (6.2) as setting $\cos(2\phi_k) = 1$. A careful reader may observe that our calculation just recovered into the case with the closed system's method as $\cos(2\phi_k) = 1$, the reason is that this kind of calculation has a correspondence between the method of the open system and the method of closed system via [65], in which η corresponds to r_k without the contribution from ϕ_k and more details can be found in Appendix A of [65]. In the later investigations, we also follow this kind of correspondence between the method of open system and the method of closed system.

In Sec. 9, we introduced the concept of Krylov complexity with the approach of open system, which is valid for the infinity, many-body, and maximal chaotic system. We then determined the Lanczos coefficient and dissipative coefficient based on the Hamiltonian. Our investigations revealed that the level of chaos in the standard case and various quantum gravitational frameworks is the same. However, in the case of non-trivial sound speed, the level of chaos is not as high as the previous two cases.

10 Evolution of Krylov complexity with approach of open system

In this section, we will investigate the Krylov complexity with the approach of open system under the thermal effects for three cases.

10.1 Evolution of standard case

With the help of Eq. (9.8), one can get the μ_1 and μ_2 for the standard case

$$|1 - \mu_1|^2 = \left(\frac{a'}{a}\right)^2, \mu_2 = k. \quad (10.1)$$

In combination with Eq. (9.14), Fig. 13 shows the evolution of Krylov complexity of standard case with thermal effect, which clearly indicates that the Krylov complexity without thermal effects will continue growing after horizon exits. But for the case with thermal effect, we could see that the Krylov complexity will grow at first and then it will decay to some very tiny values (not zero) whose trend is consistent with [9], but it is not matching our previous research [65]. This phenomenon occurs because the dissipation coefficient is always multiplied by the thermal effect ($\mu_2 \mathcal{K}$) in the equation of Krylov complexity (9.14), the higher values of temperature will speed up the dissipation process, meanwhile we have concluded that the inflationary period is already a strong dissipative system via [65]. Based on these factors, the Krylov complexity will saturate to some constant values even in inflation.

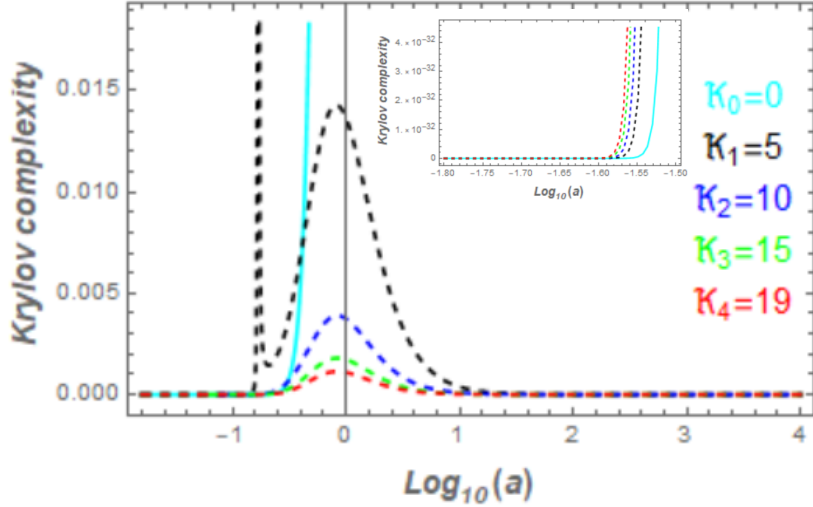


Figure 13. The numerical solutions of Krylov complexity with the open system’s method in terms of $\log_{10} a$. We have set $\mathcal{K} = 0$, $\mathcal{K} = 5$, $\mathcal{K} = 10$ and $\mathcal{K} = 0.08$ for the standard case. Our plots adopt $H = 1$ and $k = 0.01$. The horizon exits occur at $\log_{10} a = -2$.

10.2 Evolution of non-trivial sound speed

The relevant quantity can be obtained from Eq. (9.8) as follows

$$|1 - \mu_1|^2 = \left(\frac{k}{2}(c_s^2 - 1)\right)^2 + \left(\frac{a'}{a}\right)^2, \mu_2 = \frac{k}{2}(c_s^2 + 1). \quad (10.2)$$

Combined with the expression of Krylov complexity in the open system with thermal effect (9.14), the evolution of Krylov complexity can be obtained in the non-trivial sound speed model. The first plot of Fig. 14 indicates that the Krylov complexity will always grow from the entire inflationary scale, but there are some peaks for the non-trivial sound speed, especially for $\xi = 0.01$. But for the other cases of the first plot, the trend is always exponentially growing without any peak. From the first plot of Fig. 14, we can see that the peak can be dubbed as a criterion for assessing whether the inflationary models have non-trivial sound speed effects or not. For other cases, we can see that the total trend is similar, where the Krylov complexity will grow first and it will decay to some very tiny values (not zero). From observations, one can straightforwardly see that the larger values of temperature, the smaller values of the Krylov complexity will decay. In light of the conclusion from Sec. 10.1, we can also see that the strong dissipative effects of inflation and high temperature will lead to this kind of saturation for the Krylov complexity.

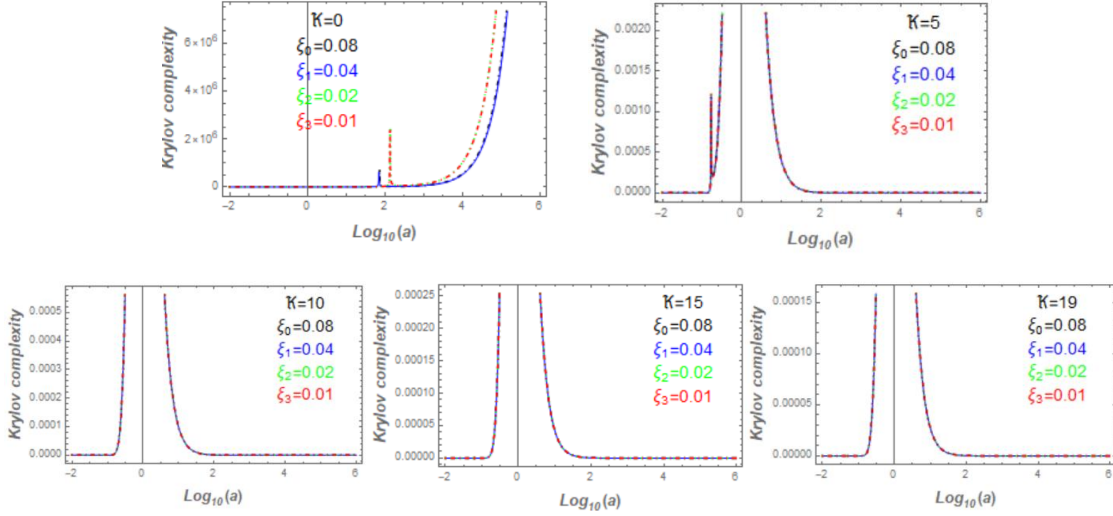


Figure 14. The numerical solutions of Krylov complexity in open system in terms of $\log_{10} a$ with for the non-trivial sound speed, the temperature parameters are set by $\mathcal{K}_1 = 0$, $\mathcal{K}_2 = 5$, $\mathcal{K}_3 = 10$, $\mathcal{K}_4 = 15$ and $\mathcal{K}_5 = 19$. And we set $\xi = 0.08$, $\xi = 0.04$, $\xi = 0.02$ and $\xi = 0.01$. Our plots adopt $H = 1$, and $k = 0.01$. The horizon exits occur at $\log_{10} a = -2$.

10.3 Evolution of modified dispersion relation

The quantity (dissipation coefficient μ_2 and Lancos coefficient $|1 - \mu_1|^2$) is available at Eq. (9.8),

$$|1 - \mu_1|^2 = \left(\frac{k}{2}(f^2 - 1)\right)^2 + \left(\frac{a'}{a}\right)^2, \mu_2 = \frac{k}{2}(f^2 + 1). \quad (10.3)$$

First, the total trend of the first plot in Fig. 15, without the thermal effect, is growing from the entire inflation, where we can see that standard case ($\alpha = 0$) will exponentially grow and the non-trivial sound speed will lead to the occurrence of peak for the Krylov complexity. Thus, the peak can also be identified with a criterion for assessing whether there is modified dispersion relation effects or not. But what factors lead to this peak, one possible reason is that the dramatically changing of background will result in this peak of Krylov complexity since μ_1 and μ_2 are the functions of scale factor a . As for other plots of Fig. 15, we can see that total trend is quite similar to Fig. 14, which it grows first and then it will decay to some tiny values. Also following the observations, we could see that the higher temperature, the smaller the tiny values. Also the strong dissipative effects and high temperature will lead to this kind of saturation.

In Sec. 10, we have investigated the Krylov complexity (9.14) for the three cases. Our numeric indicates that the Krylov complexity will always grow from the entire inflationary scale when the thermal effect is vanishing. But there are peaks of Krylov complexity by taking the non-trivial sound speed and modified dispersion into account. Our analysis reveals that the dramatic change of background will lead to the occurrence of peaks in

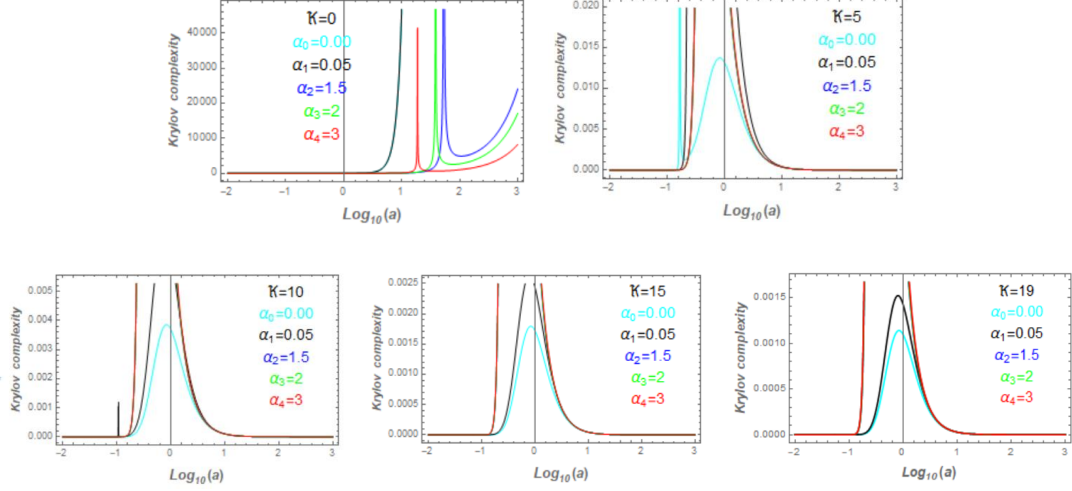


Figure 15. The numerical solutions of Krylov complexity in open system in terms of $\log_{10} a$ with $\mathcal{K}_1 = 0$, $\mathcal{K}_2 = 5$, $\mathcal{K}_3 = 10$, $\mathcal{K}_4 = 15$ and $\mathcal{K}_5 = 19$. And we set $\alpha = 0, 0.05, 1.5, 2$, and 3 . Our plots adopt $H = 1$, $k = 0.01$ and $\frac{k_{ph}}{M} = 1.5$. The horizon exits occur at $\log_{10} a = -2$.

Krylov complexity. Meanwhile, this kind of peak happens after the horizon exits, we could expect that the decoherence will highly impact the evolution of Krylov complexity, where [95] mentioned that decoherence will lead to the saturation of Krylov complexity in an open system. As for the case with the thermal effects, the biggest difference comes via that the Krylov complexity will decay to some very tiny values (not zero), and we found that the higher temperature will lead to the Krylov complexity decaying to some smaller values. Our analysis reveals that that the strong dissipative effects of inflation and high temperature will lead to this kind of saturation after the decay of Krylov complexity, even in inflation. Our previous research [65] showed that the total trend of Krylov complexity with the approach of an open system is always growing although there are some peaks at small scales, thus we could discover that our current research is more realistic once taking the thermal effects into account.

11 K-entropy with the approach of open system

We use the wave function (9.13) and the definition of K-entropy $S_K = -\sum_{n=0}^{\infty} |\phi_n|^2 \ln |\phi_n|^2$ to obtain the resulting formula as follows,

$$\begin{aligned}
 S_K = & -\frac{\operatorname{sech}^2 \eta}{[(1 + \mu_2 \tanh \eta)^2 - \mathcal{A}]^2} \\
 & \cdot \{[(1 + \mu_2 \tanh \eta)^2 - \mathcal{A}] \ln \operatorname{sech}^2 \tau + \mathcal{A} \ln \mathcal{A} - (1 + \mu_2 \tanh \eta)^2 \ln (1 + \mu_2 \tanh \eta)\} ,
 \end{aligned} \tag{11.1}$$

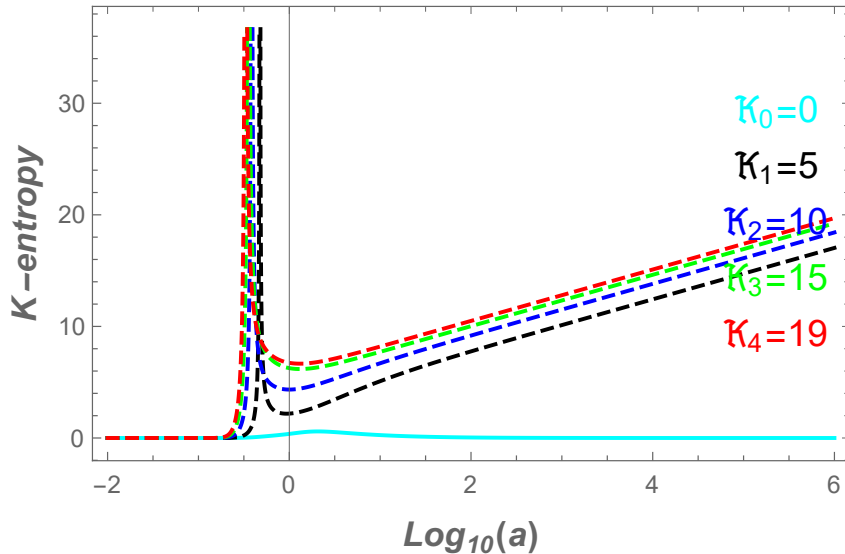


Figure 16. The numerical solutions of K-entropy in open system in terms of $\log_{10} a$ for the standard case. The temperature parameters are set with $\mathcal{K}_0 = 0$, $\mathcal{K}_1 = 5$, $\mathcal{K}_2 = 10$, $\mathcal{K}_3 = 15$ and $\mathcal{K}_4 = 19$. Our plots adopt $H = 1$, and $k = 0.01$. The horizon exits occur at $\log_{10} a = -2$.

where $\mathcal{A} = |1 - \mu_1^2|[\mathcal{K}^2 + 2\mathcal{K} \tanh \eta(\mu_2 \mathcal{K} - 1) + \tanh^2 \eta(\mu_2 \mathcal{K} - 1)^2]$ and the calculation details can be found in Sec. E. When there is no thermal effect ($\mathcal{K} = 0$), $\mathcal{A} = |1 - \mu_1^2| \tanh^2 \eta$, K-entropy becomes

$$S_K = - \frac{\text{sech}^2 \eta}{[(1 + \mu_2 \tanh \eta)^2 - |1 - \mu_1^2| \tanh^2 \eta]^2} \cdot [((1 + \mu_2 \tanh \eta)^2 - |1 - \mu_1^2| \tanh^2 \eta) \ln \text{sech}^2 - (1 + \mu_2 \tanh \eta)^2 \ln(1 + \mu_2 \tanh \eta)^2 + |1 - \mu_1^2| \tanh^2 \eta \ln |1 - \mu_1^2| \tanh^2 \eta], \quad (11.2)$$

which is consistent with Ref. [65], indicating that previous research results can be replicated when the thermal effect is ignored. From this kind of calculation, we have tested the validity of wave function (9.13). Next, we will proceed with the evolution for the K-entropy.

11.1 K-entropy of standard case

Following the Eqs. (10.1) and (11.1), we can give the numeric of K-entropy in Fig. 16, which clearly shows that the K-entropy will saturate to some tiny values as $\mathcal{K} = 0$. But for the cases with thermal effect, one could see that K-entropy will increase linearly after some peaks. The K-entropy denotes the chaos of one dynamical system, we could see that the hotter universe, the more chaotic the universe. The total trend is similar to the K-entropy in the closed system's method via Fig. 6. However, one can observe that there are peaks for the cases with thermal effect in Fig. 16, thus we conclude that the temperature leads to this kind of peaks.

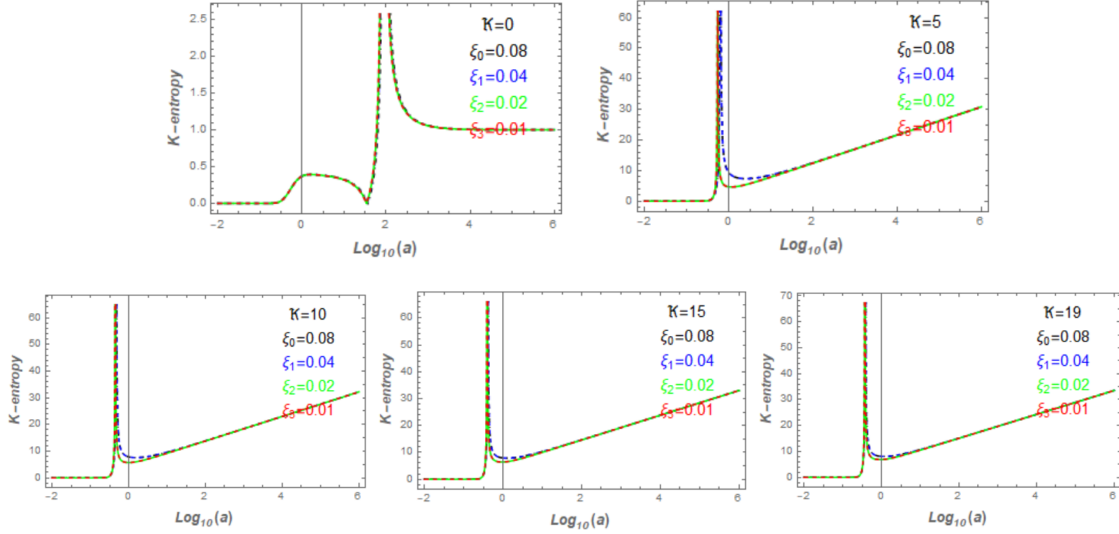


Figure 17. The numerical solutions of K-entropy in open system in terms of $\log_{10} a$ with for the non-trivial sound speed, the temperature parameters are set by $\mathcal{K}_1 = 0$, $\mathcal{K}_2 = 5$, $\mathcal{K}_3 = 10$, $\mathcal{K}_4 = 15$ and $\mathcal{K}_5 = 19$. And we set $\xi = 0.08$, $\xi = 0.04$, $\xi = 0.02$ and $\xi = 0.01$. Our plots adopt $H = 1$, and $k = 0.01$. The horizon exits occur at $\log_{10} a = -2$.

11.2 K-entropy of non-trivial sound speed

Following Eqs. (10.2) and (11.1), we can give the numeric of K-entropy for the non-trivial sound speed as shown in Fig. 17. Once taking the non-trivial sound speed into account, we can see that the evolution for the first plot of Fig. 17 shows a more colorful evolution compared with the standard case. The first plot shows that there is one oscillation after the horizon exits, then it will grow rapidly to some peak values and then it will decay into unity, which indicates the chaos of the universe will remain the same after inflation. But this situation will change dramatically when taking the thermal effects into account. The other plots of Fig. 17 clearly show the trend is quite similar to each other, which shows it has a peak after the horizon exits, and then K-entropy will grow linearly. Consequently, we could conclude that the hotter the universe, the more chaotic the universe.

11.3 K-entropy of modified dispersion relation

Together with Eqs. (10.3) and (11.1), the figure about the K-entropy of the modified dispersion relation is shown in Fig 18. The analysis can be divided into two parts: one is with thermal effect and another one is without thermal effects. For the first one ($\mathcal{K} = 0$), we could see that the K-entropy will show the same trend in the first plot of Fig. 18, there are two peaks for the K-entropy, and then it will decay into the unity as the same in Sec. 11.2. Once taking the thermal effects into account, we could see that there is one peak after the horizon exits and then it will grow linearly. Through a simple observation, we could

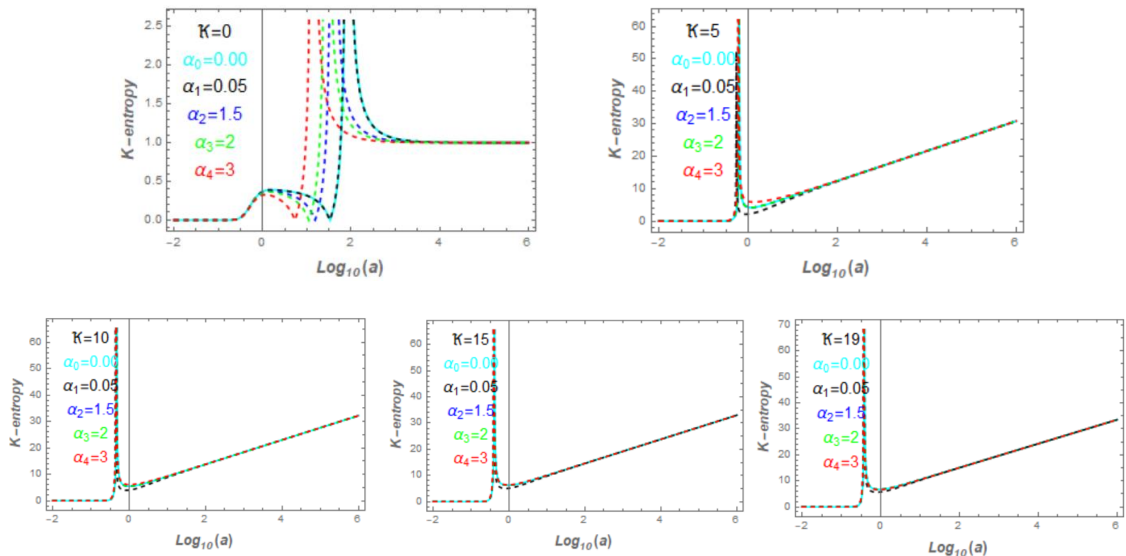


Figure 18. The numerical solutions of K-entropy in open system in terms of $\log_{10} a$ with $\mathcal{K}_1 = 0$, $\mathcal{K}_2 = 5$, $\mathcal{K}_3 = 10$, $\mathcal{K}_4 = 15$ and $\mathcal{K}_5 = 19$ for the modified dispersion relation. And we set $\alpha = 0, 0.05, 1.5, 2$, and 3 . Our plots adopt $H = 1$, $k = 0.01$ and $\frac{k_{ph}}{M} = 1.5$. The horizon exits occur at $\log_{10} a = -2$.

see that as the temperature increases, the more growth for the K-entropy, which denotes the hotter the universe, the more chaotic the universe. As for the peak of the K-entropy, it is also related to the temperature.

In Sec. 11, we demonstrated that the K-entropy can be calculated using the method via [65], which confirms the validity of wave function (9.13). We then investigated the behavior of K-entropy after the horizon exits for all cases, and found that it experiences peaks. In the absence of thermal effects, the K-entropy eventually decays to unity, which may seem counter-intuitive. However, when thermal effects are taken into account, the K-entropy grows linearly after the peak. Our research further indicates that the hotter the universe, the more chaotic it becomes.

12 Summary and outlook

The concept of complexity is becoming increasingly important in high-energy physics. Inflation provides a natural platform for high-energy physics, resulting in the cosmological collider, particle generation, and more. Additionally, inflation causes significant changes in the universe's background, making the study of complexity during inflation particularly significant. There are three standard methods for calculating complexity: the circuit complexity based on the geometrical method, the method utilizing information geometry, and the Krylov complexity. The Krylov complexity is free of ambiguities compared with other two. To compare, we calculate the circuit complexity and Krylov complexity of the cur-

vature perturbation in inflation to highlight the differences between them. The choice of wave function is another crucial aspect. The original method for measuring complexity in inflation uses the two-mode squeezed state. However, since inflation has high temperature, we use the two-mode squeezed state with thermal effect to explore complexity during inflation. Finally, most inflationary models are valid for our investigations as many quantum gravitational frameworks can lead to the modified dispersion relation and the non-trivial sound speed.

Due to the importance of inflation and thermal state, we systematically investigate the Krylov complexity and circuit complexity, especially for the Krylov complexity using the approach of closed system and method of open system together. Here, we summarize the obtained results.

(a) In this work, we have obtained the two-mode squeezed state with thermal effect as shown in Eq. (2.9). In Sec. 3 introduced the Krylov complexity and Lanczos algorithm with the approach of a closed system. Sec. 4 gives three cases: the standard case (single-field inflation), the case of non-trivial sound speed, and the case of the modified dispersion relation, where our analysis will be valid for most inflationary models since many various quantum gravitational framework could lead to this kind of non-trivial sound speed and modified dispersion relation. Based on these, we obtained the evolution of squeezed parameters $r_k(\eta)$ and $\phi_k(\eta)$ in Sec. 5. In light of their numerical solution, we found that the evolution of Krylov complexity is distinctive as taking the thermal effects, where the Krylov complexity will decrease after the horizon exits from the entire inflationary period since the evolution of Krylov complexity without thermal effects is mainly determined by ϕ_k not r_k as shown in Figs. 3, 4 and 5. But as for the case without the thermal effects, our numeric indicates that Krylov complexity is always increasing for three cases, where the formation of PBH and various gravitational frameworks could speed up the increase of Krylov complexity. Furthermore, we also investigate the K-entropy under Eq. (2.9). Figs. 6, 7 and 8 show that K-entropy is enhancing from the entire inflationary period and also tell that the higher values of temperature, the more values of K-entropy it becomes. Due to the chaotic nature of entropy, we could conclude that the hotter the universe, the more chaotic the universe will become. We discover that the evolution of the Krylov complexity and K-entropy is almost impossible for distinguishing the three cases once taking the thermal effects into account, thus our discussion is quite universal for the inflationary models.

(b) Based on the numeric of ϕ_k and r_k for the three cases, we also investigate the circuit complexity in Sec. 8. Being different from the definition of Krylov complexity, the computation of circuit complexity relies on the choice of the parametric manifold. This kind of choice leads to the different evolution of circuit complexity compared with Krylov complexity confirmed by our numeric as shown in Figs. 9, 10, 11. From these three figures, one can see that the total trend of circuit complexity from the whole inflation is increasing whether there are thermal effects or not. The main features are about the scrambling time defined as the circuit complexity begins to increase and the Lyapunov index is dubbed as the slope of complexity when complexity becomes linear. By these two definitions, we can see that the scrambling time is shorter with increasing the temperature but the

Lyapunov index will be enlarged as increasing the temperature. Due to the chaotic nature of the Lyapunov index, we could conclude that the chaos will be larger by enhancing the temperature in the case of non-trivial sound speed and modified dispersion relation. But for the standard case, the chaos is more or less remaining the same. To compare, we could see that the evolution of circuit complexity is not highly related to the temperature just from r_k , which leads to the growth of the total trend of circuit complexity. From this point, we can see that the Krylov complexity could show more features of system since its definition is unique, thus we could see that the advantage of Krylov complexity.

(c) To better describe the chaotic feature, we utilized the approach with the open system to investigate the Krylov complexity. Sec. 9 generalized the Lanczos algorithm following from [66]. We found that the Lanczos coefficient and dissipation coefficient are determined by their corresponding Hamiltonian, where Lanczos coefficient $b_n \propto n$ means that our universe is the infinity, many-body, and maximal chaotic system. Due to its nature, we could construct the wave function as shown in Eq. (9.13) in light of our previous work [65]. As for the situation without thermal effects, the numeric shows the Krylov complexity is growing from the entire inflationary period, but there are some peaks in the case of non-trivial sound speed and modified dispersion relation. Our analysis reveals that the dramatic changing of background would lead to this kind of peak. Since the peaks occur after the horizon, we could expect the decoherence will highly impact the Krylov complexity as [95] mentioned. For the situation within the thermal effects, the Krylov will eventually decay into some very tiny values (not zero) after the peaks, which is consistent with [96]. From [65], we already know that inflation is a strong dissipative system. Combined with this point, our investigations reveal that the strong dissipative effects and high temperature could lead to this kind of saturation after the peaks. For completeness, we also study the K-entropy in light of (9.13), in which all cases would experience the peaks. In the absence of thermal effects, the K-entropy will decay into the unity. Once taking the thermal effects into account, we found that the K-entropy will grow linearly after the peaks, meanwhile Figs. 16, 17 and 18 indicates that the hotter the universe, the more chaotic it becomes.

From the summary, we could see a complete physical picture of the evolution of complexity in the inflationary period. First, it will grow until to some peak values, and then it will decay into some tiny values. As for K-entropy, it reveals that the hotter the universe, the more chaotic it becomes. Although we have obtained the evolution of complexity in inflation, there are still lots of ideas worth exploring. Here, we list several problems for future research.

Firstly, our research is only focusing on the inflationary period. Thus, one can naturally extends our analysis into the matter domination (MD) or radiation domination (RD) periods, where the contribution from the inflationary potential cannot be ignored due to the violation of slow-roll condition. Another aspect is that the formula of scale factor a is different which will lead to the distinctive evolution of complexity, including the Krylov complexity and circuit complexity. Consequently, we can give a complete evolution of complexity in the whole early universe, including the inflation, RD and MD.

Secondly, Refs. [92, 93, 97] have indicated that the universe is an open system, which incorporates the non-Hermitian Hamiltonian. However, the corresponding Hamiltonian

(4.9), (4.9) and (4.17) for the three cases are all Hermitian since we only expand in their corresponding action upon to the second order in terms of Muhanov-Sasaki variable v . For obtaining the non-Hermitian Hamiltonian, we can expand the corresponding action into the third order, even higher order in terms of v . Another way for obtaining the non-Hermitian Hamiltonian, we can take the potential of inflation in RD and MD which has the interaction term between the inflaton and another field since the violation of slow-roll condition.

Thirdly, as the curvature perturbation moves from the quantum level to the classical level, decoherence will significantly impact its complexity evolution. To address this, we can expand the action into higher orders and obtain the corresponding Lindbladian, which can cause minimal decoherence [98]. By considering decoherence and Lindbladian, we can build a comprehensive physical picture of the complexity of curvature perturbation throughout the early universe, encompassing the inflation, MD, and RD eras. Additionally, the current research particularly focus on the single field, thus we could extend our investigation into the multi-field inflation [99–102] and $f(R)$ gravity [103–105], which could test the geometrical effects of field space and higher order of R (Ricci scalar) for the Krylov complexity and K-entropy.

Acknowledgments

LH and TL are supported by NSFC grant NO. 12165009, Hunan Natural Science Foundation NO. 2023JJ30487 and NO. 2022JJ40340.

A Wave function with thermal effect

In this appendix, we will derive the two-mode squeezed state with thermal effect, its original definition comes via [81]

$$|\psi_R\rangle = \exp[\mathcal{K}(\hat{c}_k^\dagger \hat{c}_{-\vec{k}}^\dagger - \hat{c}_{-\vec{k}} \hat{c}_k)] |0; 0\rangle_{\vec{k}, -\vec{k}}. \quad (\text{A.1})$$

This wave function is obtained by acting the squeezing operator $\hat{S}_k(\mathcal{K}, \frac{\pi}{2})$ on the ground state $|00\rangle_{\vec{k}, -\vec{k}}$, the thermal squeezing operator is

$$\hat{S}_k(\mathcal{K}, \frac{\pi}{2}) = \exp[\mathcal{K}(\hat{c}_k^\dagger \hat{c}_{-\vec{k}}^\dagger - \hat{c}_{-\vec{k}} \hat{c}_k)]. \quad (\text{A.2})$$

Being armed with this operator, we can write down the two-mode squeezed thermal wave function as

$$|\psi_T\rangle = \hat{S}_k(r_k, \phi_k) \hat{R}_k(\theta_k) \hat{S}_k(\mathcal{K}, \frac{\pi}{2}) |0; 0\rangle_{\vec{k}, -\vec{k}} \quad (\text{A.3})$$

where

$$\hat{S}_k(r_k, \phi_k) = \exp[r_k(\eta)(e^{-2i\phi_k(\eta)} \hat{c}_{-\vec{k}} \hat{c}_k - e^{2i\phi_k(\eta)} \hat{c}_k^\dagger \hat{c}_{-\vec{k}}^\dagger)], \quad (\text{A.4})$$

$$\hat{R}_k(\theta_k) = \exp[-i\theta_k(\eta)(\hat{c}_{-\vec{k}} \hat{c}_k^\dagger + \hat{c}_k^\dagger \hat{c}_{-\vec{k}})]. \quad (\text{A.5})$$

Thus, we can obtain

$$\begin{aligned}
|\psi_T\rangle &= \exp[r_k(\eta)(e^{-2i\phi_k(\eta)}\hat{c}_{\vec{k}}\hat{c}_{-\vec{k}} - e^{2i\phi_k(\eta)}\hat{c}_{\vec{k}}^\dagger\hat{c}_{-\vec{k}}^\dagger)] \\
&\quad \cdot \exp[-i\theta_k(\eta)(\hat{c}_{\vec{k}}\hat{c}_{\vec{k}}^\dagger + \hat{c}_{-\vec{k}}^\dagger\hat{c}_{-\vec{k}})] \\
&\quad \cdot \exp[\mathcal{K}(\hat{c}_{\vec{k}}^\dagger\hat{c}_{-\vec{k}}^\dagger - \hat{c}_{\vec{k}}\hat{c}_{-\vec{k}})] |00\rangle_{\vec{k},-\vec{k}}
\end{aligned} \tag{A.6}$$

where we use $\hat{c}_{\vec{k}}\hat{c}_{\vec{k}}^\dagger |00\rangle_{\vec{k},-\vec{k}} = |00\rangle_{\vec{k},-\vec{k}}$ and $\hat{c}_{-\vec{k}}^\dagger\hat{c}_{-\vec{k}} |00\rangle_{\vec{k},-\vec{k}} = 0$, next, we could obtain

$$\begin{aligned}
|\psi_T\rangle &= \exp(-i\theta_k) \exp[r_k(\eta)(e^{-2i\phi_k(\eta)}\hat{c}_{\vec{k}}\hat{c}_{-\vec{k}} - e^{2i\phi_k(\eta)}\hat{c}_{\vec{k}}^\dagger\hat{c}_{-\vec{k}}^\dagger)] \exp[\mathcal{K}(\hat{c}_{\vec{k}}^\dagger\hat{c}_{-\vec{k}}^\dagger - \hat{c}_{\vec{k}}\hat{c}_{-\vec{k}})] |0; 0\rangle_{\vec{k},-\vec{k}} \\
&= \exp(-i\theta_k) \exp(-r_k(\eta)e^{2i\phi_k(\eta)}\hat{c}_{\vec{k}}^\dagger\hat{c}_{-\vec{k}}^\dagger) \exp[(-2 \ln \cosh r_k) \cdot \frac{\hat{c}_{\vec{k}}\hat{c}_{\vec{k}}^\dagger + \hat{c}_{-\vec{k}}^\dagger\hat{c}_{-\vec{k}}}{2}] \\
&\quad \cdot \exp(\mathcal{K}e^{2i\phi_k(\eta)}\hat{c}_{\vec{k}}^\dagger\hat{c}_{-\vec{k}}^\dagger) \cdot \exp(-\mathcal{K}e^{2i\phi_k(\eta)}\hat{c}_{\vec{k}}\hat{c}_{-\vec{k}}) \cdot 1 |0; 0\rangle_{\vec{k},-\vec{k}} \\
&= \exp(-i\theta_k) \exp(-r_k(\eta)e^{2i\phi_k(\eta)}\hat{c}_{\vec{k}}^\dagger\hat{c}_{-\vec{k}}^\dagger) \exp[(-2 \ln \cosh r_k) \cdot \frac{\hat{c}_{\vec{k}}\hat{c}_{\vec{k}}^\dagger + \hat{c}_{-\vec{k}}^\dagger\hat{c}_{-\vec{k}}}{2}] \\
&\quad \cdot \exp(\mathcal{K}e^{-2i\phi_k(\eta)}\hat{c}_{\vec{k}}^\dagger\hat{c}_{-\vec{k}}^\dagger) \cdot 1 \cdot 1 |0; 0\rangle_{\vec{k},-\vec{k}} \\
&= \exp(-i\theta_k) \exp(-r_k(\eta)e^{2i\phi_k(\eta)}\hat{c}_{\vec{k}}^\dagger\hat{c}_{-\vec{k}}^\dagger) \exp(\mathcal{K}e^{2i\phi_k(\eta)}\hat{c}_{\vec{k}}^\dagger\hat{c}_{-\vec{k}}^\dagger) \exp[(-\ln \cosh r_k)\hat{c}_{\vec{k}}\hat{c}_{\vec{k}}^\dagger] |0; 0\rangle_{\vec{k},-\vec{k}} \\
&= \exp(-i\theta_k) \exp(-\ln \cosh r_k) \exp(-r_k(\eta)e^{2i\phi_k(\eta)}\hat{c}_{\vec{k}}^\dagger\hat{c}_{-\vec{k}}^\dagger) \exp(\mathcal{K}e^{2i\phi_k(\eta)}\hat{c}_{\vec{k}}^\dagger\hat{c}_{-\vec{k}}^\dagger) |0; 0\rangle_{\vec{k},-\vec{k}}
\end{aligned} \tag{A.7}$$

During the derivation of Eq. (A.7), we have used the following transformation,

$$\begin{cases} \frac{-e^{2i\phi_k} \sinh \beta}{\cosh \beta} = -e^{2i\phi_k} \tanh r_k \\ \frac{e^{2i\phi_k} \sinh \beta}{\cosh \beta} = e^{-2i\phi_k} \tanh r_k, \beta^2 = r_k^2 \end{cases} \tag{A.8}$$

$|\psi_T\rangle$ will become

$$\begin{aligned}
|\psi_T\rangle &= \frac{e^{-i\theta_k}}{\cosh r_k} \exp(-\tanh r_k(\eta)e^{2i\phi_k(\eta)}\hat{c}_{\vec{k}}^\dagger\hat{c}_{-\vec{k}}^\dagger) \exp(\mathcal{K}e^{2i\phi_k(\eta)}\hat{c}_{\vec{k}}^\dagger\hat{c}_{-\vec{k}}^\dagger) |0; 0\rangle_{\vec{k},-\vec{k}} \\
&= \frac{e^{-i\theta_k}}{\cosh r_k} \exp[(\mathcal{K} - \tanh r_k(\eta)e^{2i\phi_k(\eta)}\hat{c}_{\vec{k}}^\dagger\hat{c}_{-\vec{k}}^\dagger)] |0; 0\rangle_{\vec{k},-\vec{k}} \\
&= \frac{e^{-i\theta_k}}{\cosh r_k} \left(\sum_{n=0}^{\infty} \frac{(\mathcal{K} - \tanh r_k e^{2i\phi_k})^n (\hat{c}_{\vec{k}}^\dagger\hat{c}_{-\vec{k}}^\dagger)^n}{n!} \right) |0; 0\rangle_{\vec{k},-\vec{k}} \\
&= \frac{e^{-i\theta_k}}{\cosh r_k} \left(\sum_{n=0}^{\infty} \frac{(\mathcal{K} - \tanh r_k e^{2i\phi_k})^n (\sqrt{n!})^2}{n!} \right) |n; n\rangle_{\vec{k},-\vec{k}} \\
&= \frac{e^{-i\theta_k}}{\cosh r_k} \sum_{n=0}^{\infty} (\mathcal{K} - \tanh r_k e^{2i\phi_k})^n |n; n\rangle_{\vec{k},-\vec{k}}.
\end{aligned} \tag{A.9}$$

Finally, we get our resulting formula of $|\psi_T\rangle$ as shown in Eq. (2.9).

B The equation of r_k and ϕ_k

In this appendix, we will derive the evolution equation of ϕ_k and r_k of thermal state (2.9) satisfying with the Schrodinger equation $i \frac{d}{d\eta} |\psi_T\rangle = \hat{H}_k |\psi_T\rangle$. We need to calculate $i \frac{d}{d\eta} |\psi_T\rangle$ and $\hat{H}_k |\psi_T\rangle$ separately. Here, we calculate the ϕ_k and r_k of the standard case as an example, the other two cases are similar. First we do the calculation as follows,

$$\begin{aligned} i \frac{d}{d\eta} |\psi_T\rangle &= i \frac{d}{d\eta} \left[\frac{e^{-i\theta_k}}{\cosh r_k} \sum_{n=0}^{\infty} (\mathcal{K} - \tanh r_k e^{2i\phi_k})^n |n; n\rangle_{\vec{k}, -\vec{k}} \right] \\ &= i \frac{d}{d\eta} \left(\frac{e^{-i\theta_k}}{\cosh r_k} \right) \sum_{n=0}^{\infty} (\mathcal{K} - \tanh r_k e^{2i\phi_k})^n |n; n\rangle_{\vec{k}, -\vec{k}} \\ &\quad + i \frac{d}{d\eta} \left[\sum_{n=0}^{\infty} (\mathcal{K} - \tanh r_k e^{2i\phi_k})^n |n; n\rangle_{\vec{k}, -\vec{k}} \right] \frac{e^{-i\theta_k}}{\cosh r_k} \end{aligned} \quad (\text{B.1})$$

And then we could obtain

$$\begin{aligned} i \frac{d}{d\eta} |\psi_T\rangle &= \frac{e^{-i\theta_k}}{\cosh r_k} (\theta'_k - ir'_k \tanh r_k) |0; 0\rangle_{\vec{k}, -\vec{k}} \\ &\quad + \frac{e^{-i\theta_k}}{\cosh r_k} (\theta'_k - ir'_k \tanh r_k) \sum_{n=1}^{\infty} (\mathcal{K} - \tanh r_k e^{2i\phi_k})^n |n; n\rangle_{\vec{k}, -\vec{k}} \\ &\quad + \frac{e^{-i\theta_k}}{\cosh r_k} (\mathcal{K} - \tanh r_k e^{2i\phi_k})^{-1} [2\phi'_k \tanh r_k e^{2i\phi_k} \\ &\quad - ir_k e^{2i\phi_k} \text{sech}^2 r_k] \sum_{n=1}^{\infty} n (\mathcal{K} - \tanh r_k e^{2i\phi_k})^n |n; n\rangle_{\vec{k}, -\vec{k}} \end{aligned} \quad (\text{B.2})$$

Then, we will implement the Hamiltonian of (4.9) acting on the $|\psi_T\rangle$,

$$\hat{H}_k |\psi_T\rangle = \frac{e^{-i\theta_k}}{\cosh r_k} \sum_{n=0}^{\infty} (\mathcal{K} - \tanh r_k e^{2i\phi_k})^n [k (\hat{c}_{-\vec{k}}^\dagger \hat{c}_{-\vec{k}} + \hat{c}_{\vec{k}} \hat{c}_{\vec{k}}^\dagger) - i \frac{z'}{z} (\hat{c}_{\vec{k}}^\dagger \hat{c}_{-\vec{k}}^\dagger - \hat{c}_{\vec{k}} \hat{c}_{-\vec{k}})] |n; n\rangle_{\vec{k}, -\vec{k}} \quad (\text{B.3})$$

After some algebra, Eq. (B.3) will become

$$\begin{aligned} \hat{H}_k |\psi_T\rangle &= \frac{e^{-i\theta_k}}{\cosh r_k} [k - i \frac{z'}{z} (\mathcal{K} - \tanh r_k e^{2i\phi_k})] |0; 0\rangle_{\vec{k}, -\vec{k}} \\ &\quad + \frac{e^{-i\theta_k}}{\cosh r_k} [k - i \frac{z'}{z} (\mathcal{K} - \tanh r_k e^{2i\phi_k})] \sum_{n=1}^{\infty} (\mathcal{K} - \tanh r_k e^{2i\phi_k})^n |n; n\rangle_{\vec{k}, -\vec{k}} \\ &\quad + \frac{e^{-i\theta_k}}{\cosh r_k} [2k + i \frac{z'}{z} (\mathcal{K} - \tanh r_k e^{2i\phi_k})^{-1} - i \frac{z'}{z} (\mathcal{K} - \tanh r_k e^{2i\phi_k})] \\ &\quad \cdot \sum_{n=1}^{\infty} n (\mathcal{K} - \tanh r_k e^{2i\phi_k})^n |n; n\rangle_{\vec{k}, -\vec{k}} \end{aligned} \quad (\text{B.4})$$

For the further calculation, we need the following relation,

$$\begin{aligned} \hat{c}_{-\vec{k}}^\dagger \hat{c}_{-\vec{k}} |n; n\rangle_{\vec{k}, -\vec{k}} &= n |n; n\rangle_{\vec{k}, -\vec{k}}; \hat{c}_{\vec{k}} \hat{c}_{\vec{k}}^\dagger |n; n\rangle_{\vec{k}, -\vec{k}} = (n+1) |n; n\rangle_{\vec{k}, -\vec{k}} \\ \hat{c}_{\vec{k}}^\dagger \hat{c}_{-\vec{k}}^\dagger |n; n\rangle_{\vec{k}, -\vec{k}} &= (n+1) |n+1; n+1\rangle_{\vec{k}, -\vec{k}}; \hat{c}_{\vec{k}} \hat{c}_{-\vec{k}} |n; n\rangle_{\vec{k}, -\vec{k}} = n |n-1; n-1\rangle_{\vec{k}, -\vec{k}}. \end{aligned} \quad (\text{B.5})$$

Compare the ground state and excited state with Eqs. (B.3) and (B.4), we obtain the following three equations

$$\frac{e^{-i\theta_k}}{\cosh r_k} (\theta'_k - ir'_k \tanh r_k) |0; 0\rangle_{\vec{k}, -\vec{k}} = \frac{e^{-i\theta_k}}{\cosh r_k} [k - i\frac{z'}{z} (\mathcal{K} - \tanh r_k e^{2i\phi_k})] |0; 0\rangle_{\vec{k}, -\vec{k}} \quad (\text{B.6})$$

$$\begin{aligned} & \frac{e^{-i\theta_k}}{\cosh r_k} (\theta'_k - ir'_k \tanh r_k) \sum_{n=1}^{\infty} (\mathcal{K} - \tanh r_k e^{2i\phi_k})^n |n; n\rangle_{\vec{k}, -\vec{k}} \\ &= \frac{e^{-i\theta_k}}{\cosh r_k} [k - i\frac{z'}{z} (\mathcal{K} - \tanh r_k e^{2i\phi_k})] \sum_{n=1}^{\infty} (\mathcal{K} - \tanh r_k e^{2i\phi_k})^n |n; n\rangle_{\vec{k}, -\vec{k}} \end{aligned} \quad (\text{B.7})$$

$$\begin{aligned} & \frac{e^{-i\theta_k}}{\cosh r_k} (\mathcal{K} - \tanh r_k e^{2i\phi_k})^{-1} [2\phi'_k \tanh r_k e^{2i\phi_k} - ir_k e^{2i\phi_k} \operatorname{sech}^2 r_k] \\ & \cdot \sum_{n=1}^{\infty} n (\mathcal{K} - \tanh r_k e^{2i\phi_k})^n |n; n\rangle_{\vec{k}, -\vec{k}} \\ &= \frac{e^{-i\theta_k}}{\cosh r_k} [2k + i\frac{z'}{z} (\mathcal{K} - \tanh r_k e^{2i\phi_k})^{-1} - i\frac{z'}{z} (\mathcal{K} - \tanh r_k e^{2i\phi_k})] \\ & \cdot \sum_{n=1}^{\infty} n (\mathcal{K} - \tanh r_k e^{2i\phi_k})^n |n; n\rangle_{\vec{k}, -\vec{k}} \end{aligned} \quad (\text{B.8})$$

Making the comparison, we could obtain the resulting equations as follows,

$$\begin{aligned} r'_k &= \frac{a'}{a} \mathcal{K} \coth r_k - \frac{a'}{a} \cos(2\phi_k) \\ \phi'_k &= k \mathcal{K} \cos(2\phi_k) \coth r_k - k + \frac{a'}{a} \sin(2\phi_k) [\coth(2r_k) - \frac{1}{2} \mathcal{K}^2 \coth r_k] \\ \theta'_k &= k - \frac{a'}{a} \sin(2\phi_k) \tanh r_k \end{aligned} \quad (\text{B.9})$$

where the third one is not needed since the circuit complexity and Krylov complexity is independent of θ_k .

C K-entropy with the approach of closed system

In this appendix, we will calculation of K-entropy in light of

$$\phi_n = \frac{e^{-i\theta_k}}{\cosh r_k} (\mathcal{K} - \tanh r_k e^{2i\phi_k})^n. \quad (\text{C.1})$$

The definition of K-entropy is from Ref. [26],

$$S_K = - \sum_{n=0}^{\infty} |\phi_n|^2 \ln |\phi_n|^2. \quad (\text{C.2})$$

First, we need to calculate $|\phi_n|^2$

$$\begin{aligned} |\phi_n|^2 &= \frac{e^{-i\theta_k}}{\cosh r_k} (\mathcal{K} - \tanh r_k e^{2i\phi_k})^n \cdot \frac{e^{i\theta_k}}{\cosh r_k} (\mathcal{K} - \tanh r_k e^{-2i\phi_k})^n \\ &= \frac{1}{\cosh^2 r_k} (\mathcal{K}^2 - 2\mathcal{K} \tanh r_k \cos 2\phi_k + \tanh^2 r_k)^n. \end{aligned} \quad (\text{C.3})$$

And then we calculate $\ln |\phi_n|^2$,

$$\begin{aligned} \ln |\phi_n|^2 &= \ln \left[\frac{1}{\cosh^2 r_k} (\mathcal{K}^2 - 2\mathcal{K} \tanh r_k \cos 2\phi_k + \tanh^2 r_k)^n \right] \\ &= n \ln (\mathcal{K}^2 - 2\mathcal{K} \tanh r_k \cos 2\phi_k + \tanh^2 r_k) - \ln \cosh^2 r_k. \end{aligned} \quad (\text{C.4})$$

Substitute Eqs. C.3 and C.4 into Eq. C.2

$$\begin{aligned} S_K &= - \sum_{n=0}^{\infty} |\phi_n|^2 \ln |\phi_n|^2 \\ &= - \sum_{n=0}^{\infty} \frac{1}{\cosh^2 r_k} x^n (n \ln x - 2 \ln \cosh r_k) \end{aligned} \quad (\text{C.5})$$

where we have set $x = \mathcal{K}^2 - 2\mathcal{K} \tanh r_k \cos 2\phi_k + \tanh^2 r_k$ for simplicity. The equation below is derived using fundamental properties of logarithmic functions.

$$S_K = \frac{2 \ln \cosh r_k}{\cosh^2 r_k} \sum_{n=0}^{\infty} x^n - \frac{\ln x}{\cosh^2 r_k} \sum_{n=0}^{\infty} n x^n \quad (\text{C.6})$$

Making use of $\sum_{n=0}^{\infty} n x^n = \frac{x}{(1-x)^2}$ and $\sum_{n=0}^{\infty} x^n = \frac{1}{1-x}$,

$$\begin{aligned} S_K &= \frac{2 \ln \cosh r_k}{\cosh^2 r_k} \frac{1}{1-x} - \frac{\ln x}{\cosh^2 r_k} \frac{x}{(1-x)^2} \\ &= \frac{2(1-x) \ln \cosh r_k - x \ln x}{\cosh^2 r_k (1-x)^2}. \end{aligned} \quad (\text{C.7})$$

Finally, we restore x into $(\mathcal{K}^2 - 2\mathcal{K} \tanh r_k \cos 2\phi_k + \tanh^2 r_k)$ and after some algebra, we could obtain its resultsing formula as follows,

$$\begin{aligned} S_K &= \frac{2 \ln \cosh r_k}{[\cosh r_k (1 - \mathcal{K}^2 + 2\mathcal{K} \tanh r_k \cos 2\phi_k - \tanh^2 r_k)]^2} \\ &\quad - \frac{(\mathcal{K}^2 - 2\mathcal{K} \tanh r_k \cos 2\phi_k + \tanh^2 r_k) \ln [\cosh_{r_k}^2 (\mathcal{K}^2 - 2\mathcal{K} \tanh r_k \cos 2\phi_k + \tanh^2 r_k)]}{[\cosh r_k (1 - \mathcal{K}^2 + 2\mathcal{K} \tanh r_k \cos 2\phi_k - \tanh^2 r_k)]^2} \end{aligned} \quad (\text{C.8})$$

D Krylov complexity with approach of open system

In an open system, we already constructed the wave function as shown in Eq. (9.13). Then, we can calculate the Krylov complexity with the help of $\sum_{n=0}^{\infty} n |\phi_n|^2$ as follows,

$$K = \sum_{n=0}^{\infty} n \left(\frac{\text{sech } \eta}{1 + \mu_2 \tanh \eta} \right)^2 |1 - \mu_1^2|^n \left(\mathcal{K} - \frac{\tanh \eta}{1 + \mu_2 \tanh \eta} \right)^{2n} \quad (\text{D.1})$$

And then we use the relation $\sum_{n=0}^{\infty} nx^n = \frac{x}{(1-x)^2}$, finally we can get the resulting formula

$$K = \frac{1}{\cosh^2 \eta} \frac{|1 - \mu_1^2| [\mathcal{K}^2 + \tanh \eta] (2\mathcal{K}^2 \mu_2 - 2\mathcal{K}) + \tanh^2 \eta (\mathcal{K} \mu_2 - 1)^2}{\{(1 + \mu_2 \tanh \eta)^2 - |1 - \mu_1^2| [\mathcal{K}^2 + \tanh \eta] (2\mathcal{K}^2 \mu_2 - 2\mathcal{K}) + \tanh^2 \eta (\mathcal{K} \mu_2 - 1)^2\}^2} \quad (\text{D.2})$$

E K-entropy with approach of open system

From Eq. 9.13, it provides the operator wave function as follows,

$$\phi_n = \frac{\text{sech } \eta}{1 + \mu_2 \tanh \eta} |1 - \mu_1^2|^{\frac{n}{2}} \left(\mathcal{K} - \frac{\tanh \eta}{1 + \mu_2 \tanh \eta} \right)^n. \quad (\text{E.1})$$

According to the definition of K-entropy $S_K = -\sum_{n=0}^{\infty} |\phi_n|^2 \ln |\phi_n|^2$, we obtain

$$\begin{aligned} S_K &= -\sum_{n=0}^{\infty} \left(\frac{\text{sech } \eta}{1 + \mu_2 \tanh \eta} \right)^2 |1 - \mu_1^2|^{2n} \left(\mathcal{K} - \frac{\tanh \eta}{1 + \mu_2 \tanh \eta} \right)^{2n} \\ &\quad \cdot \ln \left[\left(\frac{\text{sech } \eta}{1 + \mu_2 \tanh \eta} \right)^2 |1 - \mu_1^2|^{2n} \left(\mathcal{K} - \frac{\tanh \eta}{1 + \mu_2 \tanh \eta} \right)^{2n} \right] \\ &= -\sum_{n=0}^{\infty} \left(\frac{\text{sech } \eta}{1 + \mu_2 \tanh \eta} \right)^2 |1 - \mu_1^2|^{2n} \left(\mathcal{K} - \frac{\tanh \eta}{1 + \mu_2 \tanh \eta} \right)^{2n} \ln \left(\frac{\text{sech } \eta}{1 + \mu_2 \tanh \eta} \right)^2 \\ &\quad - \sum_{n=0}^{\infty} n \left(\frac{\text{sech } \eta}{1 + \mu_2 \tanh \eta} \right)^2 |1 - \mu_1^2|^{2n} \left(\mathcal{K} - \frac{\tanh \eta}{1 + \mu_2 \tanh \eta} \right)^{2n} \ln |1 - \mu_1^2| \\ &\quad - \sum_{n=0}^{\infty} n \left(\frac{\text{sech } \eta}{1 + \mu_2 \tanh \eta} \right)^2 |1 - \mu_1^2|^{2n} \left(\mathcal{K} - \frac{\tanh \eta}{1 + \mu_2 \tanh \eta} \right)^{2n} \ln \left(\mathcal{K} - \frac{\tanh \eta}{1 + \mu_2 \tanh \eta} \right)^2. \end{aligned} \quad (\text{E.2})$$

Then, we can divide the K-entropy into three parts:

$$S_{K_1} = -\sum_{n=0}^{\infty} \left(\frac{\text{sech } \eta}{1 + \mu_2 \tanh \eta} \right)^2 |1 - \mu_1^2|^{2n} \left(\mathcal{K} - \frac{\tanh \eta}{1 + \mu_2 \tanh \eta} \right)^{2n} \ln \left(\frac{\text{sech } \eta}{1 + \mu_2 \tanh \eta} \right)^2 \quad (\text{E.3})$$

$$S_{K_2} = -\sum_{n=0}^{\infty} n \left(\frac{\text{sech } \eta}{1 + \mu_2 \tanh \eta} \right)^2 |1 - \mu_1^2|^{2n} \left(\mathcal{K} - \frac{\tanh \eta}{1 + \mu_2 \tanh \eta} \right)^{2n} \ln |1 - \mu_1^2| \quad (\text{E.4})$$

$$S_{K_3} = -\sum_{n=0}^{\infty} n \left(\frac{\text{sech } \eta}{1 + \mu_2 \tanh \eta} \right)^2 |1 - \mu_1^2|^{2n} \left(\mathcal{K} - \frac{\tanh \eta}{1 + \mu_2 \tanh \eta} \right)^{2n} \ln \left(\mathcal{K} - \frac{\tanh \eta}{1 + \mu_2 \tanh \eta} \right)^2 \eta \quad (\text{E.5})$$

First, we calculate S_{K_1}

$$\begin{aligned} S_{K_1} &= -\sum_{n=0}^{\infty} \left(\frac{\text{sech } \eta}{1 + \mu_2 \tanh \eta} \right)^2 |1 - \mu_1^2|^{2n} \left(\mathcal{K} - \frac{\tanh \eta}{1 + \mu_2 \tanh \eta} \right)^{2n} \ln \left(\frac{\text{sech } \eta}{1 + \mu_2 \tanh \eta} \right)^2 \\ &= -\left(\frac{\text{sech } \eta}{1 + \mu_2 \tanh \eta} \right)^2 \ln \left(\frac{\text{sech } \eta}{1 + \mu_2 \tanh \eta} \right)^2 \sum_{n=0}^{\infty} [|1 - \mu_1^2| \left(\mathcal{K} - \frac{\tanh \eta}{1 + \mu_2 \tanh \eta} \right)^2]^n \\ &= -\left(\frac{\text{sech } \eta}{1 + \mu_2 \tanh \eta} \right)^2 \ln \left(\frac{\text{sech } \eta}{1 + \mu_2 \tanh \eta} \right)^2 \\ &\quad \cdot \sum_{n=0}^{\infty} [|1 - \mu_1^2| \frac{\mathcal{K}^2 + 1 + \tanh \eta (2\mu_2 \mathcal{K}^2 - 2\mathcal{K}) + \tanh^2 \eta (\mu_2^2 \mathcal{K}^2 - 2\mu_2 \mathcal{K} + 1)}{(1 + \mu_2 \tanh \eta)^2}]^n. \end{aligned} \quad (\text{E.6})$$

And then making use of $\sum_{n=0}^{\infty} x^n = \frac{1}{1-x}$, we can obtain

$$S_{K_1} = -\frac{\operatorname{sech}^2 \eta \ln \left(\frac{\operatorname{sech} \eta}{1+\mu_2 \tanh \eta} \right)^2}{(1 + \mu_2 \tanh \eta)^2 - |1 - \mu_1^2| [\mathcal{K}^2 + 2\mathcal{K} \tanh \eta (\mu_2 \mathcal{K} - 1) + \tanh^2 \eta (\mu_2 \mathcal{K} - 1)^2]}.$$
(E.7)

Similar to S_{K_2} and S_{K_3} , we could obtain

$$S_{K_2} = -\frac{\operatorname{sech}^2 \eta |1 - \mu_1^2| [\mathcal{K}^2 + 2\mathcal{K} \tanh \eta (\mu_2 \mathcal{K} - 1) + \tanh^2 \eta (\mu_2 \mathcal{K} - 1)^2] \ln |1 - \mu_1^2|}{\left\{ (1 + \mu_2 \tanh \eta)^2 - |1 - \mu_1^2| [\mathcal{K}^2 + 2\mathcal{K} \tanh \eta (\mu_2 \mathcal{K} - 1) + \tanh^2 \eta (\mu_2 \mathcal{K} - 1)^2] \right\}^2}$$
(E.8)

and

$$S_{K_3} = -\frac{\operatorname{sech}^2 \eta |1 - \mu_1^2| [\mathcal{K}^2 + 2\mathcal{K} \tanh \eta (\mu_2 \mathcal{K} - 1) + \tanh^2 \eta (\mu_2 \mathcal{K} - 1)^2] \ln \left(\mathcal{K} - \frac{\tanh \eta}{1+\mu_2 \tanh \eta} \right)^2}{\left\{ (1 + \mu_2 \tanh \eta)^2 - |1 - \mu_1^2| [\mathcal{K}^2 + 2\mathcal{K} \tanh \eta (\mu_2 \mathcal{K} - 1) + \tanh^2 \eta (\mu_2 \mathcal{K} - 1)^2] \right\}^2}$$
(E.9)

For convenience, we set

$$\mathcal{A} = |1 - \mu_1^2| [\mathcal{K}^2 + 2\mathcal{K} \tanh \eta (\mu_2 \mathcal{K} - 1) + \tanh^2 \eta (\mu_2 \mathcal{K} - 1)^2]$$
(E.10)

then S_K can be rewritten as

$$\begin{aligned} S_K &= S_{K_1} + S_{K_2} + S_{K_3} \\ &= -\frac{\operatorname{sech}^2 \eta \ln \left(\frac{\operatorname{sech} \eta}{1+\mu_2 \tanh \eta} \right)^2}{(1 + \mu_2 \tanh \eta)^2 - \mathcal{A}} - \frac{\operatorname{sech}^2 \eta \mathcal{A} \ln |1 - \mu_1^2|}{[(1 + \mu_2 \tanh \eta)^2 - \mathcal{A}]^2} - \frac{\operatorname{sech}^2 \eta \mathcal{A} \ln \left(\mathcal{K} - \frac{\tanh \eta}{1+\mu_2 \tanh \eta} \right)^2}{[(1 + \mu_2 \tanh \eta)^2 - \mathcal{A}]^2} \\ &= -\frac{\operatorname{sech}^2 \eta [(1 + \mu_2 \tanh \eta)^2 - \mathcal{A}] \ln \left(\frac{\operatorname{sech} \eta}{1+\mu_2 \tanh \eta} \right)^2}{[(1 + \mu_2 \tanh \eta)^2 - \mathcal{A}]^2} \\ &\quad - \frac{\operatorname{sech}^2 \eta \mathcal{A} \ln |1 - \mu_1^2| + \operatorname{sech}^2 \eta \mathcal{A} \ln \left(\mathcal{K} - \frac{\tanh \eta}{1+\mu_2 \tanh \eta} \right)^2}{[(1 + \mu_2 \tanh \eta)^2 - \mathcal{A}]^2} \end{aligned}$$
(E.11)

After some simple algebra, we can get the final resulting formula as follows,

$$\begin{aligned} S_K &= -\frac{\operatorname{sech}^2 \eta}{[(1 + \mu_2 \tanh \eta)^2 - \mathcal{A}]^2} \\ &\quad \cdot \left\{ [(1 + \mu_2 \tanh \eta)^2 - \mathcal{A}] \ln \operatorname{sech}^2 \eta + \mathcal{A} \ln \mathcal{A} - (1 + \mu_2 \tanh \eta)^2 \ln (1 + \mu_2 \tanh \eta)^2 \right\}. \end{aligned}$$
(E.12)

References

- [1] D. Stanford and L. Susskind, Phys. Rev. D **90** (2014) no.12, 126007 doi:10.1103/PhysRevD.90.126007 [arXiv:1406.2678 [hep-th]].
- [2] T. Hartman and J. Maldacena, JHEP **05** (2013), 014 doi:10.1007/JHEP05(2013)014 [arXiv:1303.1080 [hep-th]].

- [3] H. Liu and S. J. Suh, Phys. Rev. Lett. **112** (2014), 011601
doi:10.1103/PhysRevLett.112.011601 [arXiv:1305.7244 [hep-th]].
- [4] S. Aaronson, [arXiv:1607.05256 [quant-ph]].
- [5] M. A. Nielsen, Quant. Inf. Comput. **6** (2006) no.3, 213-262 doi:10.26421/QIC6.3-2
[arXiv:quant-ph/0502070 [quant-ph]].
- [6] M. A. Nielsen, M. R. Dowling, M. Gu and A. C. Doherty, Science **311** (2006) no.5764,
1133-1135 doi:10.1126/science.1121541 [arXiv:quant-ph/0603161 [quant-ph]].
- [7] M. R. Dowling and M. A. Nielsen, Quant. Inf. Comput. **8** (2008) no.10, 0861-0899
doi:10.26421/QIC8.10-1 [arXiv:quant-ph/0701004 [quant-ph]].
- [8] S. Chapman, M. P. Heller, H. Marrochio and F. Pastawski, Phys. Rev. Lett. **120** (2018)
no.12, 121602 doi:10.1103/PhysRevLett.120.121602 [arXiv:1707.08582 [hep-th]].
- [9] D. E. Parker, X. Cao, A. Avdoshkin, T. Scaffidi and E. Altman, Phys. Rev. X **9** (2019) no.4,
041017 doi:10.1103/PhysRevX.9.041017 [arXiv:1812.08657 [cond-mat.stat-mech]].
- [10] V. S. Viswanath, Gerhard Müller, The recursion method: application to many body
dynamics. Vol. 23. Springer Science and Business Media, 1994.
- [11] S. E. Aguilar-Gutierrez and A. Rolph, Phys. Rev. D **109** (2024) no.8, L081701
doi:10.1103/PhysRevD.109.L081701 [arXiv:2311.04093 [hep-th]].
- [12] R. Jefferson and R. C. Myers, JHEP **10** (2017), 107 doi:10.1007/JHEP10(2017)107
[arXiv:1707.08570 [hep-th]].
- [13] A. Bhattacharyya, A. Shekar and A. Sinha, JHEP **10** (2018), 140
doi:10.1007/JHEP10(2018)140 [arXiv:1808.03105 [hep-th]].
- [14] M. Guo, J. Hernandez, R. C. Myers and S. M. Ruan, JHEP **10** (2018), 011
doi:10.1007/JHEP10(2018)011 [arXiv:1807.07677 [hep-th]].
- [15] S. Chapman, J. Eisert, L. Hackl, M. P. Heller, R. Jefferson, H. Marrochio and R. C. Myers,
SciPost Phys. **6** (2019) no.3, 034 doi:10.21468/SciPostPhys.6.3.034 [arXiv:1810.05151
[hep-th]].
- [16] L. Hackl and R. C. Myers, JHEP **07** (2018), 139 doi:10.1007/JHEP07(2018)139
[arXiv:1803.10638 [hep-th]].
- [17] D. W. F. Alves and G. Camilo, JHEP **06** (2018), 029 doi:10.1007/JHEP06(2018)029
[arXiv:1804.00107 [hep-th]].
- [18] H. A. Camargo, P. Caputa, D. Das, M. P. Heller and R. Jefferson, Phys. Rev. Lett. **122**
(2019) no.8, 081601 doi:10.1103/PhysRevLett.122.081601 [arXiv:1807.07075 [hep-th]].
- [19] T. Ali, A. Bhattacharyya, S. Shajidul Haque, E. H. Kim and N. Moynihan, Phys. Lett. B
811 (2020), 135919 doi:10.1016/j.physletb.2020.135919 [arXiv:1811.05985 [hep-th]].
- [20] R. Khan, C. Krishnan and S. Sharma, Phys. Rev. D **98** (2018) no.12, 126001
doi:10.1103/PhysRevD.98.126001 [arXiv:1801.07620 [hep-th]].
- [21] D. A. Roberts and B. Yoshida, JHEP **04** (2017), 121 doi:10.1007/JHEP04(2017)121
[arXiv:1610.04903 [quant-ph]].
- [22] V. Balasubramanian, M. Decross, A. Kar and O. Parrikar, JHEP **01** (2020), 134
doi:10.1007/JHEP01(2020)134 [arXiv:1905.05765 [hep-th]].

- [23] T. Ali, A. Bhattacharyya, S. S. Haque, E. H. Kim, N. Moynihan and J. Murugan, Phys. Rev. D **101** (2020) no.2, 026021 doi:10.1103/PhysRevD.101.026021 [arXiv:1905.13534 [hep-th]].
- [24] R. Q. Yang and K. Y. Kim, JHEP **05** (2020), 045 doi:10.1007/JHEP05(2020)045 [arXiv:1906.02052 [hep-th]].
- [25] A. Bhattacharyya, W. Chemissany, S. Shajidul Haque and B. Yan, Eur. Phys. J. C **82** (2022) no.1, 87 doi:10.1140/epjc/s10052-022-10035-3 [arXiv:1909.01894 [hep-th]].
- [26] J. L. F. Barbón, E. Rabinovici, R. Shir and R. Sinha, JHEP **10** (2019), 264 doi:10.1007/JHEP10(2019)264 [arXiv:1907.05393 [hep-th]].
- [27] W. Mück and Y. Yang, Nucl. Phys. B **984** (2022), 115948 doi:10.1016/j.nuclphysb.2022.115948 [arXiv:2205.12815 [hep-th]].
- [28] E. Rabinovici, A. Sánchez-Garrido, R. Shir and J. Sonner, JHEP **06** (2021), 062 doi:10.1007/JHEP06(2021)062 [arXiv:2009.01862 [hep-th]].
- [29] S. K. Jian, B. Swingle and Z. Y. Xian, JHEP **03** (2021), 014 doi:10.1007/JHEP03(2021)014 [arXiv:2008.12274 [hep-th]].
- [30] S. He, P. H. C. Lau, Z. Y. Xian and L. Zhao, JHEP **12** (2022), 070 doi:10.1007/JHEP12(2022)070 [arXiv:2209.14936 [hep-th]].
- [31] D. Patramanis, PTEP **2022** (2022) no.6, 063A01 doi:10.1093/ptep/ptac081 [arXiv:2111.03424 [hep-th]].
- [32] X. Cao, J. Phys. A **54** (2021) no.14, 144001 doi:10.1088/1751-8121/abe77c [arXiv:2012.06544 [cond-mat.stat-mech]].
- [33] F. B. Trigueros and C. J. Lin, SciPost Phys. **13** (2022) no.2, 037 doi:10.21468/SciPostPhys.13.2.037 [arXiv:2112.04722 [cond-mat.dis-nn]].
- [34] R. Heveling, J. Wang and J. Gemmer, Phys. Rev. E **106** (2022) no.1, 014152 doi:10.1103/PhysRevE.106.014152 [arXiv:2203.00533 [cond-mat.stat-mech]].
- [35] A. Dymarsky and M. Smolkin, Phys. Rev. D **104** (2021) no.8, L081702 doi:10.1103/PhysRevD.104.L081702 [arXiv:2104.09514 [hep-th]].
- [36] P. Caputa and S. Datta, JHEP **12** (2021), 188 [erratum: JHEP **09** (2022), 113] doi:10.1007/JHEP12(2021)188 [arXiv:2110.10519 [hep-th]].
- [37] P. Caputa and S. Liu, Phys. Rev. B **106** (2022) no.19, 195125 doi:10.1103/PhysRevB.106.195125 [arXiv:2205.05688 [hep-th]].
- [38] A. Dymarsky and A. Gorsky, Phys. Rev. B **102** (2020) no.8, 085137 doi:10.1103/PhysRevB.102.085137 [arXiv:1912.12227 [cond-mat.stat-mech]].
- [39] B. Bhattacharjee, X. Cao, P. Nandy and T. Pathak, JHEP **05** (2022), 174 doi:10.1007/JHEP05(2022)174 [arXiv:2203.03534 [quant-ph]].
- [40] K. B. Huh, H. S. Jeong and J. F. Pedraza, [arXiv:2312.12593 [hep-th]].
- [41] J. Erdmenger, S. K. Jian and Z. Y. Xian, JHEP **08** (2023), 176 doi:10.1007/JHEP08(2023)176 [arXiv:2303.12151 [hep-th]].
- [42] K. Hashimoto, K. Murata, N. Tanahashi and R. Watanabe, JHEP **11** (2023), 040 doi:10.1007/JHEP11(2023)040 [arXiv:2305.16669 [hep-th]].

- [43] M. J. Vasli, K. Babaei Velni, M. R. Mohammadi Mozaffar, A. Mollabashi and M. Alishahiha, *Eur. Phys. J. C* **84** (2024) no.3, 235 doi:10.1140/epjc/s10052-024-12609-9 [arXiv:2307.08307 [hep-th]].
- [44] A. Gill, K. Pal, K. Pal and T. Sarkar, *Phys. Rev. B* **109** (2024) no.10, 104303 doi:10.1103/PhysRevB.109.104303 [arXiv:2311.07892 [quant-ph]].
- [45] B. Bhattacharjee, P. Nandy and T. Pathak, *JHEP* **01** (2024), 094 doi:10.1007/JHEP01(2024)094 [arXiv:2311.00753 [quant-ph]].
- [46] K. Adhikari, S. Choudhury and A. Roy, *Nucl. Phys. B* **993** (2023), 116263 doi:10.1016/j.nuclphysb.2023.116263 [arXiv:2204.02250 [hep-th]].
- [47] T. Q. Loc, [arXiv:2402.07980 [hep-th]].
- [48] P. Caputa, H. S. Jeong, S. Liu, J. F. Pedraza and L. C. Qu, [arXiv:2402.09522 [hep-th]].
- [49] R. Basu, A. Ganguly, S. Nath and O. Parrikar, [arXiv:2402.13694 [hep-th]].
- [50] R. Sasaki, [arXiv:2403.06391 [quant-ph]].
- [51] P. Caputa and K. Kutak, [arXiv:2404.07657 [hep-ph]].
- [52] A. Sahu, [arXiv:2404.09464 [quant-ph]].
- [53] B. Bhattacharjee, S. Sur and P. Nandy, *Phys. Rev. B* **106** (2022) no.20, 205150 doi:10.1103/PhysRevB.106.205150 [arXiv:2208.05503 [quant-ph]].
- [54] J. Kim, J. Murugan, J. Olle and D. Rosa, *Phys. Rev. A* **105** (2022) no.1, L010201 doi:10.1103/PhysRevA.105.L010201 [arXiv:2109.05301 [quant-ph]].
- [55] L. Chen, B. Mu, H. Wang and P. Zhang, [arXiv:2404.08207 [quant-ph]].
- [56] K. Adhikari, S. Choudhury, H. N. Pandya and R. Srivastava, *Symmetry* **15** (2023) no.3, 664 doi:10.3390/sym15030664 [arXiv:2108.10334 [gr-qc]].
- [57] S. Choudhury, S. Chowdhury, N. Gupta, A. Mishara, S. P. Selvam, S. Panda, G. D. Pasquino, C. Singha and A. Swain, *Symmetry* **13** (2021) no.7, 1301 doi:10.3390/sym13071301 [arXiv:2012.10234 [hep-th]].
- [58] P. Bhargava, S. Choudhury, S. Chowdhury, A. Mishara, S. P. Selvam, S. Panda and G. D. Pasquino, *SciPost Phys. Core* **4** (2021), 026 doi:10.21468/SciPostPhysCore.4.4.026 [arXiv:2009.03893 [hep-th]].
- [59] J. L. Lehners and J. Quintin, *Phys. Rev. D* **103** (2021) no.6, 063527 doi:10.1103/PhysRevD.103.063527 [arXiv:2012.04911 [hep-th]].
- [60] A. Bhattacharyya, S. Das, S. Shajidul Haque and B. Underwood, *Phys. Rev. D* **101** (2020) no.10, 106020 doi:10.1103/PhysRevD.101.106020 [arXiv:2001.08664 [hep-th]].
- [61] L. H. Liu and A. C. Li, *Phys. Dark Univ.* **37** (2022), 101123 doi:10.1016/j.dark.2022.101123 [arXiv:2102.12014 [gr-qc]].
- [62] A. c. Li, X. F. Li, D. f. Zeng and L. H. Liu, *Phys. Dark Univ.* **43** (2024), 101422 doi:10.1016/j.dark.2024.101422 [arXiv:2102.12939 [gr-qc]].
- [63] T. Li and L. H. Liu, [arXiv:2309.01595 [gr-qc]].
- [64] K. Adhikari and S. Choudhury, *Fortsch. Phys.* **70** (2022) no.12, 2200126 doi:10.1002/prop.202200126 [arXiv:2203.14330 [hep-th]].

- [65] T. Li and L. H. Liu, JHEP **04** (2024), 123 doi:10.1007/JHEP04(2024)123 [arXiv:2401.09307 [hep-th]].
- [66] A. Bhattacharya, P. Nandy, P. P. Nath and H. Sahu, JHEP **12** (2022), 081 doi:10.1007/JHEP12(2022)081 [arXiv:2207.05347 [quant-ph]].
- [67] A. Kar, L. Lamprou, M. Rozali and J. Sully, JHEP **01** (2022), 016 doi:10.1007/JHEP01(2022)016 [arXiv:2106.02046 [hep-th]].
- [68] J. Wang, H. Yu and P. Wu, [arXiv:2212.01512 [gr-qc]].
- [69] Y. F. Cai and X. Zhang, Phys. Rev. D **80** (2009), 043520 doi:10.1103/PhysRevD.80.043520 [arXiv:0906.3341 [astro-ph.CO]].
- [70] Y. F. Cai, X. Tong, D. G. Wang and S. F. Yan, Phys. Rev. Lett. **121** (2018) no.8, 081306 doi:10.1103/PhysRevLett.121.081306 [arXiv:1805.03639 [astro-ph.CO]].
- [71] M. Alishahiha, E. Silverstein and D. Tong, Phys. Rev. D **70** (2004), 123505 doi:10.1103/PhysRevD.70.123505 [arXiv:hep-th/0404084 [hep-th]].
- [72] E. Silverstein and D. Tong, Phys. Rev. D **70** (2004), 103505 doi:10.1103/PhysRevD.70.103505 [arXiv:hep-th/0310221 [hep-th]].
- [73] C. Chen, X. H. Ma and Y. F. Cai, Phys. Rev. D **102** (2020) no.6, 063526 doi:10.1103/PhysRevD.102.063526 [arXiv:2003.03821 [astro-ph.CO]].
- [74] A. Achucarro, J. O. Gong, S. Hardeman, G. A. Palma and S. P. Patil, JHEP **05** (2012), 066 doi:10.1007/JHEP05(2012)066 [arXiv:1201.6342 [hep-th]].
- [75] C. Armendariz-Picon and E. A. Lim, JCAP **12** (2003), 002 doi:10.1088/1475-7516/2003/12/002 [arXiv:astro-ph/0307101 [astro-ph]].
- [76] C. Armendariz-Picon, JCAP **10** (2006), 010 doi:10.1088/1475-7516/2006/10/010 [arXiv:astro-ph/0606168 [astro-ph]].
- [77] J. Magueijo, Phys. Rev. D **79** (2009), 043525 doi:10.1103/PhysRevD.79.043525 [arXiv:0807.1689 [gr-qc]].
- [78] J. Martin and R. H. Brandenberger, Phys. Rev. D **63** (2001), 123501 doi:10.1103/PhysRevD.63.123501 [arXiv:hep-th/0005209 [hep-th]].
- [79] N. Arkani-Hamed, H. C. Cheng, M. A. Luty and S. Mukohyama, JHEP **05** (2004), 074 doi:10.1088/1126-6708/2004/05/074 [arXiv:hep-th/0312099 [hep-th]].
- [80] M. Bojowald, H. Hernandez, M. Kagan, P. Singh and A. Skirzewski, Phys. Rev. Lett. **98** (2007), 031301 doi:10.1103/PhysRevLett.98.031301 [arXiv:astro-ph/0611685 [astro-ph]].
- [81] Y. Takahashi and H. Umezawa, Int. J. Mod. Phys. B **10** (1996), 1755-1805 doi:10.1142/S0217979296000817
- [82] A. Ferraro, S. Olivares and M. G. A. Paris, [arXiv:quant-ph/0503237 [quant-ph]].
- [83] Weedbrook, C. Pirandola, S. García-Patrón, R. Cerf, N. J. Ralph, T. C. Shapiro, J. H. and Lloyd, S, *American Physical Society* 84.2 (2012): 621. doi: 10.1103/RevModPhys.84.621.
- [84] L. P. Grishchuk and Y. V. Sidorov, Phys. Rev. D **42** (1990), 3413-3421 doi:10.1103/PhysRevD.42.3413
- [85] C. Armendariz-Picon, T. Damour and V. F. Mukhanov, Phys. Lett. B **458** (1999), 209-218 doi:10.1016/S0370-2693(99)00603-6 [arXiv:hep-th/9904075 [hep-th]].

- [86] J. Garriga and V. F. Mukhanov, *Phys. Lett. B* **458** (1999), 219-225
doi:10.1016/S0370-2693(99)00602-4 [arXiv:hep-th/9904176 [hep-th]].
- [87] A. H. Guth, *Phys. Rev. D* **23** (1981), 347-356 doi:10.1103/PhysRevD.23.347
- [88] E. Kiritsis and G. Kofinas, *Nucl. Phys. B* **821** (2009), 467-480
doi:10.1016/j.nuclphysb.2009.05.005 [arXiv:0904.1334 [hep-th]].
- [89] G. Calcagni, *JHEP* **09** (2009), 112 doi:10.1088/1126-6708/2009/09/112 [arXiv:0904.0829 [hep-th]].
- [90] A. Albrecht, P. Ferreira, M. Joyce and T. Prokopec, *Phys. Rev. D* **50** (1994), 4807-4820
doi:10.1103/PhysRevD.50.4807 [arXiv:astro-ph/9303001 [astro-ph]].
- [91] T. Ali, A. Bhattacharyya, S. Shajidul Haque, E. H. Kim and N. Moynihan, *JHEP* **04** (2019), 087 doi:10.1007/JHEP04(2019)087 [arXiv:1810.02734 [hep-th]].
- [92] C. Cheung, P. Creminelli, A. L. Fitzpatrick, J. Kaplan and L. Senatore, *JHEP* **03** (2008), 014 doi:10.1088/1126-6708/2008/03/014 [arXiv:0709.0293 [hep-th]].
- [93] L. Kofman, A. D. Linde and A. A. Starobinsky, *Phys. Rev. Lett.* **73** (1994), 3195-3198
doi:10.1103/PhysRevLett.73.3195 [arXiv:hep-th/9405187 [hep-th]].
- [94] A. Bhattacharya, P. Nandy, P. P. Nath and H. Sahu, *JHEP* **12** (2023), 066
doi:10.1007/JHEP12(2023)066 [arXiv:2303.04175 [quant-ph]].
- [95] A. Bhattacharyya, T. Hanif, S. S. Haque and A. Paul, *Phys. Rev. D* **107** (2023) no.10, 106007 doi:10.1103/PhysRevD.107.106007 [arXiv:2210.09268 [hep-th]].
- [96] B. Bhattacharjee, X. Cao, P. Nandy and T. Pathak, *JHEP* **03** (2023), 054
doi:10.1007/JHEP03(2023)054 [arXiv:2212.06180 [quant-ph]].
- [97] L. Kofman, A. D. Linde and A. A. Starobinsky, *Phys. Rev. D* **56** (1997), 3258-3295
doi:10.1103/PhysRevD.56.3258 [arXiv:hep-ph/9704452 [hep-ph]].
- [98] C. P. Burgess, R. Holman, G. Kaplanek, J. Martin and V. Vennin, *JCAP* **07** (2023), 022
doi:10.1088/1475-7516/2023/07/022 [arXiv:2211.11046 [hep-th]].
- [99] L. H. Liu and W. L. Xu, *Chin. Phys. C* **44** (2020) no.8, 085103
doi:10.1088/1674-1137/44/8/085103 [arXiv:1911.10542 [astro-ph.CO]].
- [100] L. H. Liu and T. Prokopec, *JCAP* **06** (2021), 033 doi:10.1088/1475-7516/2021/06/033
[arXiv:2005.11069 [astro-ph.CO]].
- [101] L. H. Liu, *Chin. Phys. C* **47** (2023) no.1, 015105 doi:10.1088/1674-1137/ac9d28
[arXiv:2107.07310 [astro-ph.CO]].
- [102] X. z. Zhang, L. h. Liu and T. Qiu, *Phys. Rev. D* **107** (2023) no.4, 043510
doi:10.1103/PhysRevD.107.043510 [arXiv:2207.07873 [hep-th]].
- [103] L. H. Liu, B. Liang, Y. C. Zhou, X. D. Liu, W. L. Xu and A. C. Li, *Phys. Rev. D* **103** (2021) no.6, 063515 doi:10.1103/PhysRevD.103.063515 [arXiv:2007.08278 [astro-ph.CO]].
- [104] L. H. Liu, doi:10.1007/s10773-018-3809-0 [arXiv:1807.00666 [gr-qc]].
- [105] L. H. Liu, T. Prokopec and A. A. Starobinsky, *Phys. Rev. D* **98** (2018) no.4, 043505
doi:10.1103/PhysRevD.98.043505 [arXiv:1806.05407 [gr-qc]].